Published for SISSA by Springer

Received: March 28, 2014
Accepted: June 3, 2014
Published: June 26, 2014

Confronting Higgcision with electric dipole moments

Kingman Cheung,[a,b] **Jae Sik Lee,**[c] **Eibun Senaha**[d] **and Po-Yan Tseng**[a]

[a] *Department of Physics, National Tsing Hua University, Hsinchu 300, Taiwan*

[b] *Division of Quantum Phases and Devices, School of Physics, Konkuk University, Seoul 143-701, Republic of Korea*

[c] *Department of Physics, Chonnam National University, 300 Yongbong-dong, Buk-gu, Gwangju, 500-757, Republic of Korea*

[d] *Department of Physics, Nagoya University, Nagoya 464-8602, Japan*

E-mail: cheung@phys.nthu.edu.tw, jslee@jnu.ac.kr, senaha@eken.phys.nagoya-u.ac.jp, d9722809@oz.nthu.edu.tw

Abstract: Current data on the signal strengths and angular spectrum of the 125.5 GeV Higgs boson still allow a CP-mixed state, namely, the pseudoscalar coupling to the top quark can be as sizable as the scalar coupling: $C_u^S \approx C_u^P = 1/2$. CP violation can then arise and manifest in sizable electric dipole moments (EDMs). In the framework of two-Higgs-doublet models, we not only update the Higgs precision (Higgcision) study on the couplings with the most updated Higgs signal strength data, but also compute all the Higgs-mediated contributions from the 125.5 GeV Higgs boson to the EDMs, and confront the allowed parameter space against the existing constraints from the EDM measurements of Thallium, neutron, Mercury, and Thorium monoxide. We found that the combined EDM constraints restrict the pseudoscalar coupling to be less than about 10^{-2}, unless there are contributions from other Higgs bosons, supersymmetric particles, or other exotic particles that delicately cancel the current Higgs-mediated contributions.

Keywords: Higgs Physics, CP violation

ArXiv ePrint: 1403.4775

doi:10.1007/JHEP06(2014)149

Contents

1 Introduction

Since the observation of a new boson at a mass around 125.5 GeV at the Large Hadron Collider (LHC) [1, 2], the most urgent mission is to investigate the properties of this new boson. There have been a large number of studies or fits of the Higgs boson couplings to the standard model (SM) particles in more or less model-independent frameworks [3–18, 20–32], in the two-Higgs doublet model (2HDM) frameworks [33–51], and in the supersymmetric frameworks [52–56]. Based on a study using a generic framework for Higgs couplings to the relevant SM particles, three of us has reported [22] that the SM Higgs boson [57–59] provides the best fit to all the most updated Higgs data from ATLAS [60–63], CMS [64–70], and Tevatron [71, 72]. In particular, the relative coupling to the gauge bosons is restricted to be close to the SM values with about a 15% uncertainty while the Yukawa couplings are only loosely constrained. Furthermore, the hypothesis of a pure CP-odd state for the new boson has been mostly ruled out by angular measurements [73, 74]. Nevertheless, there is still a large room for the possibility of a CP-mixed state [19, 22].

If the Higgs boson is a CP-mixed state, it can simultaneously couple to the scalar and pseudoscalar fermion bilinears as follows:

$$\mathcal{L}_{H\bar{f}f} = -g_f\, H\, \bar{f}\left(g^S_{H\bar{f}f} + i g^P_{H\bar{f}f}\gamma_5\right) f\,, \tag{1.1}$$

where $g_f = gm_f/2M_W = m_f/v$ with $f = u, d, l$ denoting the up- and down-type quarks and charged leptons collectively. We will show that non-zero values of the products proportional to $g^S_{H\bar{f}f} \times g^P_{H\bar{f}^{(\prime)}f^{(\prime)}}$ and $g^P_{H\bar{f}f} \times g_{HVV}$ signal CP violation as manifested in nonzero values for electric dipole moments (EDMs).[1] The non-observation of the Thallium (^{205}Tl) [75], neutron (n) [76], Mercury (^{199}Hg) [77], and thorium monoxide (ThO) [78] EDMs provide remarkably tight bounds on CP violation. The EDM constraints in light of the recent Higgs data were studied in refs. [79, 80]. Strictly speaking, only the Higgs couplings to the third-generation fermions such as the top and bottom quarks and tau leptons are relevant to the current Higgs data. On the other hand, the EDM experiments mainly involve the first-generation fermions. Therefore, it is impossible to relate the Higgs precision (Higgcision) constraints to EDMs in a completely model-independent fashion without specifying the relations among the generations, except for the Weinberg operator. In most of the models studied in literature, however, the Higgs couplings to the third-generation fermions are related to those of the first-generation in a model-dependent way. In this work, to be specific, we study the contributions of the observed 125.5 GeV "Higgs" boson (H) to EDMs in the framework of 2HDMs.

The paper is organized as follows. In section 2 we briefly describe ingredients in the framework of 2HDMs we are working with and present the 2HDM Higgcision fit to the most updated Higgs data. For notation and more details of the 2HDMs we refer to ref. [51]. Section 3 is devoted to the synopsis of EDMs. In section 4 we present our numerical results, and summarize our findings and draw conclusions in section 5.

2 Two Higgs doublet models

In ref. [51], neglecting the charged Higgs contribution to the loop-induced Higgs couplings to two photons, it was shown that the Higgcision studies in 2HDM framework can be performed with a minimum of three parameters, given by

$$C^S_u \equiv g^S_{H\bar{t}t}\,; \qquad C^P_u \equiv g^P_{H\bar{t}t}\,; \qquad C_v \equiv g_{HVV}\,, \tag{2.1}$$

where $H = h_i$ denotes the candidate of the 125.5 GeV Higgs among the three neutral Higgs bosons $h_{1,2,3}$ in 2HDMs without further specifying which one the observed one is. The mixing between the mass eigenstates $h_{1,2,3}$ and the electroweak eigenstates ϕ_1, ϕ_2, a is described by an orthogonal matrix O as in

$$(\phi_1, \phi_2, a)^T_\alpha = O_{\alpha j}(h_1, h_2, h_3)^T_j\,. \tag{2.2}$$

Once the three parameters C^S_u, C^P_u, and C_v are given, the H couplings to the SM fermions are completely determined as shown in table 1.[2] Note the relations

$$O_{\phi_1 i} = \pm\big[1 - (O_{\phi_2 i})^2 - (O_{ai})^2\big]^{1/2}, \qquad O_{\phi_2 i} = s_\beta\, C^S_u\,, \qquad O_{ai} = -t_\beta\, C^P_u \tag{2.3}$$

[1]Here, g_{HVV} denotes a generic Higgs coupling to the massive vector bosons in the interaction $\mathcal{L}_{HVV} = g\,M_W\, g_{HVV}\big(W^+_\mu W^{-\mu} + \frac{1}{2\cos^2\theta_W}\, Z_\mu Z^\mu\big)\, H$.

[2]One may use $\tan\beta$ as an input parameter instead of C_v. Then, the coupling C_v is given by $C_v = c_\beta O_{\phi_1 i} + s_\beta O_{\phi_2 i}$.

2HDM I	$C_d^S = C_u^S$	$C_l^S = C_u^S$	$C_d^P = -C_u^P$	$C_l^P = -C_u^P$
2HDM II	$C_d^S = \frac{O_{\phi_1 i}}{c_\beta}$	$C_l^S = \frac{O_{\phi_1 i}}{c_\beta}$	$C_d^P = t_\beta^2 C_u^P$	$C_l^P = t_\beta^2 C_u^P$
2HDM III	$C_d^S = C_u^S$	$C_l^S = \frac{O_{\phi_1 i}}{c_\beta}$	$C_d^P = -C_u^P$	$C_l^P = t_\beta^2 C_u^P$
2HDM IV	$C_d^S = \frac{O_{\phi_1 i}}{c_\beta}$	$C_l^S = C_u^S$	$C_d^P = t_\beta^2 C_u^P$	$C_l^P = -C_u^P$

Table 1. The couplings $C_{d,l}^{S,P} \equiv g_{H\bar{d}d,H\bar{l}l}^{S,P}$ as functions of $C_u^{S,P}$ and $\tan\beta$ in the four types of 2HDMs, see ref. [51] for details of conventions in 2HDMs.

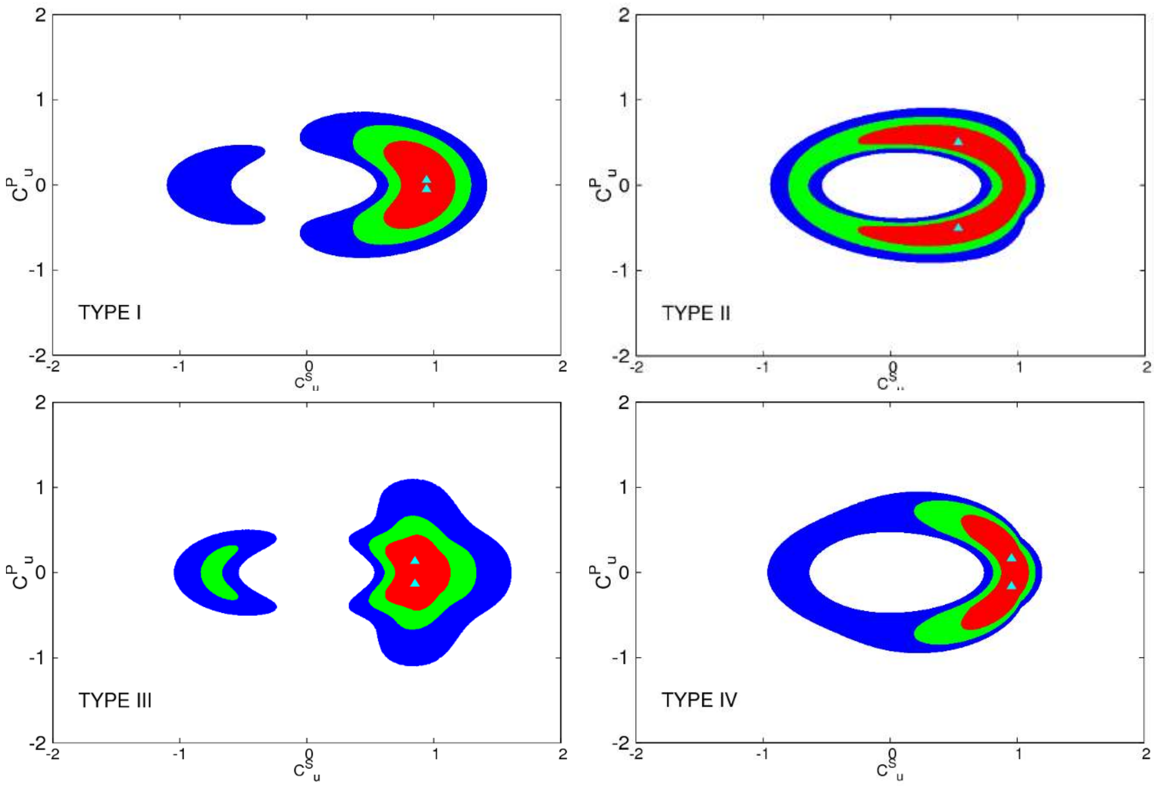

Figure 1. The confidence-level regions of the fit to the most updated Higgs data by varying C_u^S, C_u^P, and C_v in the plane of C_u^S vs C_u^P for Type I–IV. The contour regions shown are for $\Delta\chi^2 \leq 2.3$ (red), 5.99 (green), and 11.83 (blue) above the minimum, which correspond to confidence levels of 68.3%, 95%, and 99.7%, respectively. The best-fit points are denoted by the triangles.

with

$$s_\beta^2 = \frac{(1-C_v^2)}{(1-C_v^2)+(C_u^S-C_v)^2+(C_u^P)^2}\,. \tag{2.4}$$

We are using the abbreviations: $s_\beta \equiv \sin\beta$, $c_\beta \equiv \cos\beta$, $t_\beta = \tan\beta$, etc, and the convention of $C_v > 0$.

In figure 1, we show the confidence-level (CL) regions of the fit to the most updated Higgs data by varying C_u^S, C_u^P, and C_v in the plane of C_u^S vs C_u^P for Type I–IV of the 2HDMs. Comparing to figure 11 in ref. [51] for the **CPV3** fit, the CL regions are mildly reduced, preferring positive C_u^S values slightly more than the negative ones, after the inclusion of the most recent results from $H \to b\bar{b}$ [62, 69, 70] and $\tau^+\tau^-$ [63, 68]. Meanwhile, we note that the maximal CP violation with $C_u^S \sim |C_u^P|$ is still possible.

3 Synopsis of EDMs

Here we closely follow the methods used in refs. [81–84] in the calculations of the 125.5-GeV Higgs-mediated contributions to the EDMs. We start by giving the relevant interaction Lagrangian as

$$\begin{aligned}\mathcal{L} = & -\frac{i}{2}\, d_f^E\, F^{\mu\nu}\, \bar{f}\, \sigma_{\mu\nu}\gamma_5\, f - \frac{i}{2}\, d_q^C\, G^{a\,\mu\nu}\, \bar{q}\, \sigma_{\mu\nu}\gamma_5 T^a\, q \\ & +\frac{1}{3}\, d^G\, f_{abc}\, G^a_{\rho\mu}\, \widetilde{G}^{b\,\mu\nu}\, G^c{}_\nu{}^\rho + \sum_{f,f'} C_{ff'}\, (\bar{f}f)(\bar{f}' i\gamma_5 f')\,,\end{aligned} \tag{3.1}$$

where $F^{\mu\nu}$ and $G^{a\,\mu\nu}$ are the electromagnetic and strong field strengths, respectively, the $T^a = \lambda^a/2$ are the generators of the $\mathrm{SU}(3)_C$ group and $\widetilde{G}^{\mu\nu} = \frac{1}{2}\epsilon^{\mu\nu\lambda\sigma} G_{\lambda\sigma}$ is the dual of the $\mathrm{SU}(3)_c$ field-strength tensor $G_{\lambda\sigma}$.

We denote the EDM of a fermion by d_f^E and the chromoelectric dipole moment (CEDM) of a quark by d_q^C. The major Higgs-mediated contribution comes from the two-loop Barr-Zee-type diagrams, labeled as

$$(d_f^E)^H = (d_f^E)^{\rm BZ}\,; \qquad (d_q^C)^H = (d_q^C)^{\rm BZ}\,, \tag{3.2}$$

the details of which will be discussed below. For the Weinberg operator, we consider the contributions from the Higgs-mediated two-loop diagrams:

$$(d^G)^H = \frac{4\sqrt{2}\, G_F\, g_s^3}{(4\pi)^4} \sum_{q=t,b} g^S_{H\bar{q}q}\, g^P_{H\bar{q}q}\, h(z_{Hq})\,, \tag{3.3}$$

where $z_{Hq} \equiv M_H^2/m_q^2$ with $M_H = 125.5\,\mathrm{GeV}$ and, for the loop function $h(z_{Hq})$, we refer to ref. [85]. We note, in passing, that $(d^G)^H$ depends on the H couplings to the third-generation quarks only. For the four-fermion operators, we consider the t-channel exchanges of the CP-mixed state H, which give rise to the CP-odd coefficients as follows [81]:

$$(C_{ff'})^H = g_f\, g_{f'}\, \frac{g^S_{H\bar{f}f}\, g^P_{H\bar{f}'f'}}{M_H^2}\,. \tag{3.4}$$

3.1 Two-loop Barr-Zee EDMs

We consider both the Barr-Zee diagrams mediated by the γ-γ-H couplings [81] and by the γ-H-Z couplings [86, 87]. More explicitly the contributions from the two-loop Higgs-mediated Barr-Zee-type diagrams can be decomposed into two parts:

$$(d_f^E)^{\rm BZ} = (d_f^E)^{\gamma H} + (d_f^E)^{ZH} \tag{3.5}$$

JHEP06(2014)149

where

$$(-Q_f)^{-1}\times\left(\frac{d_f^E}{e}\right)^{\gamma H} = \sum_{q=t,b}\left\{\frac{3\alpha_{\rm em}^2\,Q_q^2\,m_f}{8\pi^2 s_W^2 M_W^2}\left[g^P_{H\bar ff}g^S_{H\bar qq}\,f(\tau_{qH})+g^S_{H\bar ff}g^P_{H\bar qq}\,g(\tau_{qH})\right]\right\}$$
$$+\frac{\alpha_{\rm em}^2\,m_f}{8\pi^2 s_W^2 M_W^2}\left[g^P_{H\bar ff}g^S_{H\tau^+\tau^-}\,f(\tau_{\tau H})+g^S_{H\bar ff}g^P_{H\tau^+\tau^-}\,g(\tau_{\tau H})\right]$$
$$-\frac{\alpha_{\rm em}^2\,m_f}{32\pi^2 s_W^2 M_W^2}\,g^P_{H\bar ff}g_{HVV}\,\mathcal{J}^\gamma_W(M_H) \tag{3.6}$$

with $\tau_{xH}=m_x^2/M_H^2$. For the loop functions $f(\tau)$ and $g(\tau)$ we refer to, for example, refs. [81, 82] and references therein. The loop function $\mathcal{J}_W^{G=\gamma,Z}(M_H)$ for the W-loop contributions is given by [88]

$$\mathcal{J}_W^G(M_H)=\frac{2M_W^2}{M_H^2-M_G^2}\left\{-\frac{1}{4}\left[\left(6-\frac{M_G^2}{M_W^2}\right)+\left(1-\frac{M_G^2}{2M_W^2}\right)\frac{M_H^2}{M_W^2}\right]\left[I_1(M_W,M_H)-I_1(M_W,M_G)\right]\right.$$
$$\left.+\left[\left(-4+\frac{M_G^2}{M_W^2}\right)+\frac{1}{4}\left(6-\frac{M_G^2}{M_W^2}\right)+\frac{1}{4}\left(1-\frac{M_G^2}{2M_W^2}\right)\frac{M_H^2}{M_W^2}\right]\left[I_2(M_W,M_H)-I_2(M_W,M_G)\right]\right\} \tag{3.7}$$

where

$$I_1(m_1,m_2)=-2\frac{m_2^2}{m_1^2}f\left(\frac{m_1^2}{m_2^2}\right),\qquad I_2(m_1,m_2)=-2\frac{m_2^2}{m_1^2}g\left(\frac{m_1^2}{m_2^2}\right). \tag{3.8}$$

We note that, for large τ, $f(\tau)\sim 13/18+(\ln\tau)/3$ and $g(\tau)\sim 1+(\ln\tau)/2$ [89]. Also, $(d_f^E)^{ZH}$ is given by

$$\left(\frac{d_f^E}{e}\right)^{ZH} = \frac{\alpha_{\rm em}^2 v_{Z\bar ff}}{16\sqrt{2}\pi^2 c_W^2 s_W^4}\,\frac{m_f}{M_W}\sum_{q=t,b}\frac{3Q_q m_q}{\sqrt{2}M_W}$$
$$\times\left[g^S_{H\bar ff}\left(v_{Z\bar qq}g^P_{H\bar qq}\right)\frac{m_q}{M_H^2}\int_0^1 {\rm d}x\frac{1}{x}J\left(r_{ZH},\frac{r_{qH}}{x(1-x)}\right)\right.$$
$$\left.+\,g^P_{H\bar ff}\left(v_{Z\bar qq}g^S_{H\bar qq}\right)\frac{m_q}{M_H^2}\int_0^1 {\rm d}x\frac{1-x}{x}J\left(r_{ZH},\frac{r_{qH}}{x(1-x)}\right)\right]$$
$$-\frac{\alpha_{\rm em}^2 v_{Z\bar ff}}{16\sqrt{2}\pi^2 c_W^2 s_W^4}\,\frac{m_f}{M_W}\,\frac{m_\tau}{\sqrt{2}M_W}$$
$$\times\left[g^S_{H\bar ff}\left(v_{Z\tau^+\tau^-}g^P_{H\tau^+\tau^-}\right)\frac{m_\tau}{M_H^2}\int_0^1 {\rm d}x\frac{1}{x}J\left(r_{ZH},\frac{r_{\tau H}}{x(1-x)}\right)\right.$$
$$\left.+\,g^P_{H\bar ff}\left(v_{Z\tau^+\tau^-}g^S_{H\tau^+\tau^-}\right)\frac{m_\tau}{M_H^2}\int_0^1 {\rm d}x\frac{1-x}{x}J\left(r_{ZH},\frac{r_{\tau H}}{x(1-x)}\right)\right]$$
$$+\frac{\alpha_{\rm em}^2\,v_{Z\bar ff}\,m_f}{32\pi^2 s_W^4 M_W^2}\,g^P_{H\bar ff}g_{HVV}\,\mathcal{J}^Z_W(M_H)\,, \tag{3.9}$$

with $r_{xy}\equiv M_x^2/M_y^2$. For the loop function $J(a,b)$ we again refer to, for example, refs. [81, 82] and references therein. The Z-boson couplings to the quarks and leptons are given by

$$\mathcal{L}_{Z\bar ff}=-g_Z\,\bar f\,\gamma^\mu\,(v_{Z\bar ff}-a_{Z\bar ff}\gamma_5)\,f\,Z_\mu \tag{3.10}$$

JHEP06(2014)149

with $v_{Z\bar{f}f} = T_{3L}^f/2 - Q_f s_W^2$ and $a_{Z\bar{f}f} = T_{3L}^f/2$ and $g_Z = g/c_W = (e/s_W)/c_W$. For the SM quarks and leptons, $T_{3L}^{u,\nu} = +1/2$ and $T_{3L}^{d,e} = -1/2$.

In addition to EDMs, the two-loop Higgs-mediated Barr-Zee graphs also generate CEDMs of the light quarks $q_l = u, d$, which take the form:

$$(d_{q_l}^C)^{\rm BZ} = -\frac{g_s\,\alpha_s\,\alpha_{\rm em}\,m_{q_l}}{16\pi^2 s_W^2 M_W^2} \sum_{q=t,b} \left[g^P_{H\bar{q}_l q_l} g^S_{H\bar{q}q}\, f(\tau_{qH}) + g^S_{H\bar{q}_l q_l} g^P_{H\bar{q}q}\, g(\tau_{qH}) \right] . \tag{3.11}$$

3.2 Observable EDMs

In this subsection, we briefly review the dependence of the Thallium, neutron, Mercury, deuteron, Radium, and thorium-monoxide EDMs on the EDMs and/or CEDMs of quarks and leptons, and on the coefficients of the dimension-six Weinberg operator and the four-fermion operators.

3.2.1 Thallium EDM

The Thallium EDM receives contributions mainly from two terms [90, 91]:

$$d_{\rm Tl}\,[e\,{\rm cm}] = -585 \cdot d_e^E\,[e\,{\rm cm}] - 8.5 \times 10^{-19}\,[e\,{\rm cm}] \cdot (C_S\,{\rm TeV}^2) + \cdots , \tag{3.12}$$

where d_e^E is the electron EDM and C_S is the coefficient of the CP-odd electron-nucleon interaction $\mathcal{L}_{C_S} = C_S\,\bar{e}i\gamma_5\,e\bar{N}N$, which is given by

$$C_S = C_{de}\frac{29\,{\rm MeV}}{m_d} + C_{se}\frac{\kappa \times 220\,{\rm MeV}}{m_s} + (0.1\,{\rm GeV})\,\frac{m_e}{v^2}\frac{g^S_{H_igg} g^P_{H\bar{e}e}}{M_H^2} \tag{3.13}$$

with $\kappa \equiv \langle N|m_s\bar{s}s|N\rangle/220\,{\rm MeV} \simeq 0.50 \pm 0.25$ and

$$g^S_{H_igg} = \sum_{q=t,b} \left\{ \frac{2\,x_q}{3} g^S_{H_i\bar{q}q} \right\} , \tag{3.14}$$

with $x_t = 1$ and $x_b = 1 - 0.25\kappa$.

3.2.2 Thorium-monoxide EDM

Similar to the Thallium EDM, the thorium-monoxide EDM is given by [92]:

$$d_{\rm ThO}\,[e\,{\rm cm}] = \mathcal{F}_{\rm ThO}\left\{ d_e^E\,[e\,{\rm cm}] + 1.6 \times 10^{-21}\,[e\,{\rm cm}]\,(C_S\,{\rm TeV}^2) \right\} + \cdots . \tag{3.15}$$

Currently, the experimental constraint is given on the quantity $|d_{\rm ThO}/\mathcal{F}_{\rm ThO}|$.

3.2.3 Neutron EDM

For the neutron EDM we take the hadronic approach with the QCD sum-rule technique. In this approach, the neutron EDM is given by [93–98]

$$\begin{aligned}
d_n &= d_n(d_q^E\,, d_q^C) + d_n(d^G) + d_n(C_{bd}) + \cdots , \\
d_n(d_q^E\,, d_q^C) &= (1.4 \pm 0.6)\,(d_d^E - 0.25\,d_u^E) + (1.1 \pm 0.5)\,e\,(d_d^C + 0.5\,d_u^C)/g_s\,, \\
d_n(d^G) &\sim \pm\,e\,(20 \pm 10)\,{\rm MeV}\,d^G, \\
d_n(C_{bd}) &\sim \pm\,e\,2.6 \times 10^{-3}\,{\rm GeV}^2 \left[\frac{C_{bd}}{m_b} + 0.75\frac{C_{db}}{m_b} \right] ,
\end{aligned} \tag{3.16}$$

where d_q^E and d_q^C should be evaluated at the electroweak (EW) scale and d^G at the 1 GeV scale, for which $d^G|_{1\,\mathrm{GeV}} \simeq (\eta^G/0.4)\, d^G|_{\mathrm{EW}} \simeq 8.5\, d^G|_{\mathrm{EW}}$ [96] taking $\eta^G = 3.4$ [99, 100]. In the numerical estimates we take the positive sign for both $d_n(d^G)$ and $d_n(C_{bd})$.

3.2.4 Mercury EDM

Using the QCD sum rules [97, 98], we estimate the Mercury EDM as

$$\begin{aligned} d_{\mathrm{Hg}}^{\mathrm{I,II,III,IV}} &= d_{\mathrm{Hg}}^{\mathrm{I,II,III,IV}}[S] + 10^{-2} d_e^E + (3.5 \times 10^{-3}\,\mathrm{GeV})\, e\, C_S \\ &\quad + (4 \times 10^{-4}\,\mathrm{GeV})\, e \left[C_P + \left(\frac{Z-N}{A} \right)_{\mathrm{Hg}} C_P' \right], \end{aligned} \tag{3.17}$$

where $d_{\mathrm{Hg}}^{\mathrm{I,II,III,IV}}[S]$ denotes the Mercury EDM induced by the Schiff moment. The parameters C_P and C_P' are the couplings of electron-nucleon interactions as in $\mathcal{L}_{C_P} = C_P\, \bar{e}e\, \bar{N} i\gamma_5 N + C_P'\, \bar{e}e\, \bar{N} i\gamma_5 \tau_3 N$ and they are given by [81]

$$\begin{aligned} C_P &\simeq -375\,\mathrm{MeV} \sum_{q=c,s,t,b} \frac{C_{eq}}{m_q}, \\ C_P' &\simeq -806\,\mathrm{MeV}\, \frac{C_{ed}}{m_d} - 181\,\mathrm{MeV} \sum_{q=c,s,t,b} \frac{C_{eq}}{m_q}. \end{aligned} \tag{3.18}$$

In this work, we take $d_{\mathrm{Hg}}^{\mathrm{I}}[S]$ for the Schiff-moment induced Mercury EDM, which is given by [83]

$$d_{\mathrm{Hg}}^{\mathrm{I}}[S] \simeq 1.8 \times 10^{-3}\, e\, \bar{g}_{\pi NN}^{(1)}/\mathrm{GeV}, \tag{3.19}$$

where

$$\begin{aligned} \bar{g}_{\pi NN}^{(1)} &= 2_{-1}^{+4} \times 10^{-12}\, \frac{(d_u^C - d_d^C)/g_s}{10^{-26}\mathrm{cm}}\, \frac{|\langle \bar{q}q \rangle|}{(225\,\mathrm{MeV})^3} \\ &\quad - 8 \times 10^{-3}\,\mathrm{GeV}^3 \left[\frac{0.5 C_{dd}}{m_d} + 3.3\kappa \frac{C_{sd}}{m_s} + (1 - 0.25\kappa) \frac{C_{bd}}{m_b} \right]. \end{aligned} \tag{3.20}$$

3.2.5 Deuteron EDM

For the deuteron EDM, we use [81, 101]:

$$\begin{aligned} d_D &\simeq -\left[5_{-3}^{+11} + (0.6 \pm 0.3) \right] e\, (d_u^C - d_d^C)/g_s \\ &\quad - (0.2 \pm 0.1)\, e\, (d_u^C + d_d^C)/g_s + (0.5 \pm 0.3)(d_u^E + d_d^E) \\ &\quad + (1 \pm 0.2) \times 10^{-2}\, e\,\mathrm{GeV}^2 \left[\frac{0.5 C_{dd}}{m_d} + 3.3\kappa \frac{C_{sd}}{m_s} + (1 - 0.25\kappa) \frac{C_{bd}}{m_b} \right] \\ &\quad \pm e\, (20 \pm 10)\,\mathrm{MeV}\, d^G. \end{aligned} \tag{3.21}$$

In the above, d^G is evaluated at the 1 GeV scale, and the coupling coefficients $g_{d,s,b}$ appearing in $C_{dd,sd,bd}$ are computed at energies 1 GeV, 1 GeV and m_b, respectively. All other EDM operators are calculated at the EW scale. In the numerical estimates we take the positive sign for d^G.

3.2.6 Radium EDM

For the EDM of ^{225}Ra, we use [83]:

$$d_{\rm Ra} \simeq d_{\rm Ra}[S] \simeq -8.7\times 10^{-2}\, e\, \bar{g}^{(0)}_{\pi NN}/{\rm GeV} + 3.5\times 10^{-1}\, e\, \bar{g}^{(1)}_{\pi NN}/{\rm GeV}, \tag{3.22}$$

where

$$\bar{g}^{(0)}_{\pi NN} = 0.4\times 10^{-12}\, \frac{(d_u^C + d_d^C)/g_s}{10^{-26}{\rm cm}}\, \frac{|\langle \bar{q}q\rangle|}{(225\,{\rm MeV})^3}\,. \tag{3.23}$$

We note that the $\bar{g}^{(1)}_{\pi NN}$ contribution to the Radium EDM is about 200 times larger than that to the Mercury EDM $d^{\rm I}_{\rm Hg}[S]$ [102].

4 Numerical analysis

The non-observation of EDMs for Thallium [75], neutron [76], Mercury [77], and thorium monoxide [78] constrains the CP-violating phases through

$$\begin{aligned} |d_{\rm Tl}| &\le d^{\rm EXP}_{\rm Tl}, & |d_{\rm n}| &\le d^{\rm EXP}_{\rm n}, \\ |d_{\rm Hg}| &\le d^{\rm EXP}_{\rm Hg}, & |d_{\rm ThO}/\mathcal{F}_{\rm ThO}| &\le d^{\rm EXP}_{\rm ThO}\,, \end{aligned} \tag{4.1}$$

with the current experimental bounds

$$\begin{aligned} d^{\rm EXP}_{\rm Tl} &= 9\times 10^{-25}\, e\,{\rm cm}\,, & d^{\rm EXP}_{\rm n} &= 2.9\times 10^{-26}\, e\,{\rm cm}\,, \\ d^{\rm EXP}_{\rm Hg} &= 3.1\times 10^{-29}\, e\,{\rm cm}\,, & d^{\rm EXP}_{\rm ThO} &= 8.7\times 10^{-29}\, e\,{\rm cm}\,. \end{aligned} \tag{4.2}$$

For the normalization of the deuteron and Radium EDMs, we have taken the projected experimental sensitivity [103] to be $d^{\rm PRJ}_{\rm D} = 3\times 10^{-27}\, e\,{\rm cm}$ and $d^{\rm PRJ}_{\rm Ra} = 1\times 10^{-27}\, e\,{\rm cm}$, respectively. The chosen value for $d^{\rm PRJ}_{\rm Ra}$ is near to a sensitivity which can be achieved in one day of data-taking [104]. On the other hand, the future Higgs-boson data may shrink the CL regions that we obtained in figure 1. Nevertheless, we have to emphasize that the combined constraint on $|C^P_u|$ from all the current EDM measurements is at the level of 10^{-2} at 95% CL without any further assumptions beyond the 125.5 GeV Higgs-mediated contributions, see eq. (4.10). The future Higgs-boson data alone cannot further reduce such a strong constraint on $|C^P_u|$ while the deuteron and Radium EDMs are capable of probing $|C^P_u| \lesssim 10^{-2}$ with the estimates of the projected sensitivities.

4.1 (C)EDMs of quarks and leptons and d^G

In this subsection, we analyze the contributions of the Higgs boson H with the mass 125.5 GeV in the 2HDM framework to

- EDMs of electron and up and down quarks: $d^E_f = (d^E_f)^{\rm BZ} = (d^E_f)^{\gamma H} + (d^E_f)^{ZH}$ with $f = e, u, d$,
- CEDMs of up and down quarks: $d^C_q = (d^C_q)^{\rm BZ}$ with $q = u, d$, and
- Coefficient of the Weinberg operator d^G,

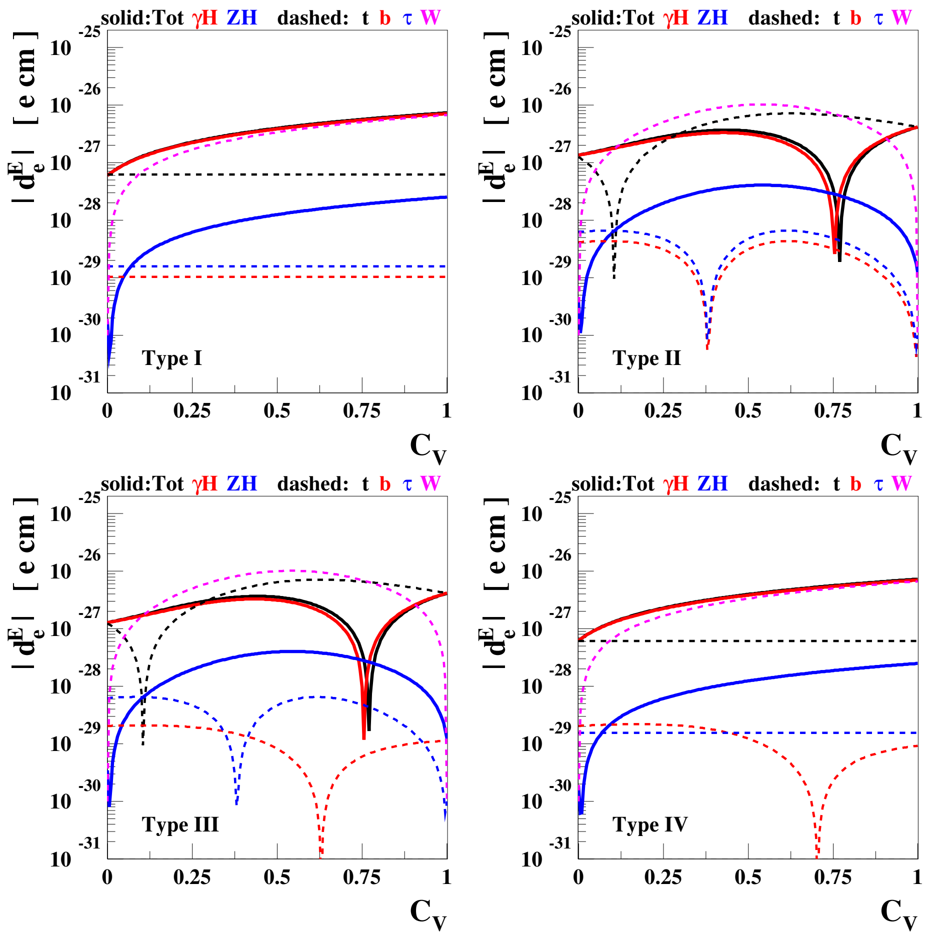

Figure 2. The absolute values of the electron EDM as functions of C_v in units of $e\,\mathrm{cm}$ when $C_u^S = C_u^P = 1/2$ for the types I–IV of 2HDMs. The red and blue solid lines are for $(d_e^E)^{\gamma H}$ and $(d_e^E)^{ZH}$, respectively, and the black solid lines are for the total sum. The constituent contributions from top, bottom, tau, and W-boson loops are denoted by the dashed black, red, blue, and magenta lines, respectively.

together with their constituent contributions, taking the benchmark point

$$C_u^S = C_u^P = 1/2\,, \tag{4.3}$$

while varying C_v.

In figure 2, we show the electron EDM as a function of C_v in units of $e\,\mathrm{cm}$ with $C_u^S = C_u^P = 1/2$ for the types I–IV of 2HDMs. The red and blue solid lines are for $(d_e^E)^{\gamma H}$ and $(d_e^E)^{ZH}$, respectively, and the black solid lines are for the total sum. The constituent contributions from the top, bottom, tau, and W-boson loops are denoted by the dashed black, red, blue, and magenta lines, respectively. In all types of 2HDMs, we observe that $(d_e^E)^{\gamma H}$, the contribution from the γ-H Barr-Zee diagram, dominates over $(d_e^E)^{ZH}$, which is suppressed by the factor $v_{Z\bar{e}e} = -1/4 + s_W^2$. Also, the W-boson loop contribution is dominant in types I and IV when $C_v \gtrsim 0.1$, and the top and W-boson loop contributions are comparable in Types II and III.

JHEP06(2014)149

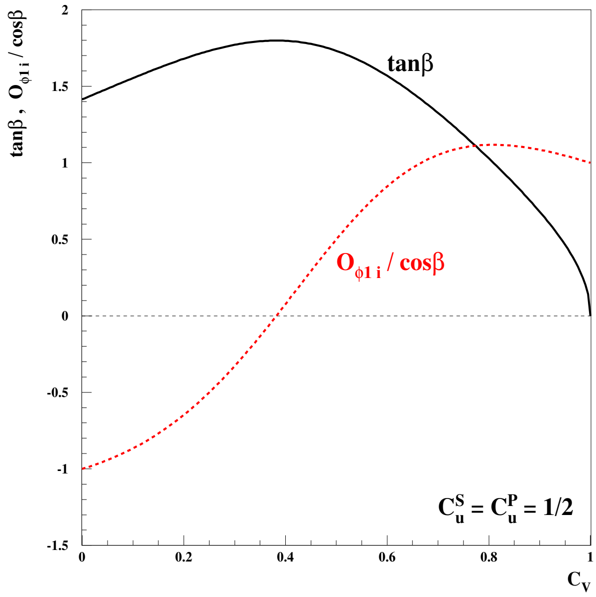

Figure 3. $\tan\beta$ and $O_{\phi_1 i}/\cos\beta$ as functions of C_v taking $C_u^S = C_u^P = 1/2$.

Keeping only the top and W-loop contributions in the γ-H Barr-Zee diagram and neglecting the Z-H Barr-Zee diagram, the electron EDM satisfies

$$\left(\frac{d_e^E}{e}\right)_{\rm I,IV} \propto \left\{\frac{16}{3}[-f(\tau_{tH})+g(\tau_{tH})]\,C_u^S + C_v\,\mathcal{J}_W^\gamma(M_H)\right\} C_u^P\,, \tag{4.4}$$
$$\left(\frac{d_e^E}{e}\right)_{\rm II,III} \propto \left\{\frac{16}{3}\left[t_\beta^2 C_u^S\,f(\tau_{tH}) + \frac{O_{\phi_1 i}}{c_\beta}\,g(\tau_{tH})\right] - t_\beta^2 C_v\,\mathcal{J}_W^\gamma(M_H)\right\} C_u^P\,,$$

for Type I, IV and II, III, respectively: see eq. (3.6). Numerically, $f(\tau_{tH}) \simeq 0.98$, $g(\tau_{tH}) \simeq 1.4$, and $\mathcal{J}_W^\gamma(M_H) \simeq 12$. We observe that the electron EDM is overall proportional to C_u^P and it flips the sign according to the change in the sign of C_u^P. The top and W contributions have the same signs, and the top-quark contributions are independent of C_v in Types I and IV. Also, note that the two top-quark contributions in Types I and IV cancel each other so that the top-quark contribution is suppressed compared to that in Types II and III. For the reference point $C_u^S = C_u^P = 1/2$, we show $\tan\beta$ and $O_{\phi_1 i}/\cos\beta$ as functions of C_v in figure 3.[3] When $C_v \gtrsim 0.4$, $O_{\phi_i 1}$ is positive and we see that the top and W contributions have the opposite signs in Types II and III, which leads to a large cancellation between the top (dashed black lines) and W (dashed magenta lines) contributions around $C_v = 0.75$ in Types II and III: see the upper-right and lower-left frames of figure 2. Since $O_{\phi_i 1} < 0$ when $C_v \lesssim 0.4$, the two top-quark contributions in Types II and III cancel each other and thus explains the dips in the constituent contributions from top loops (black dashed lines) around $C_v = 0.1$ in Types II and III.

In figure 4, we show the absolute values of the up-quark EDM as a function of C_v in units of $e\,$cm with $C_u^S = C_u^P = 1/2$ for Types I–IV of 2HDMs. The labeling of the lines is

[3]Note that $\sin\beta = 0$ when $C_v = 1$ for non-zero C_u^P independent of C_u^S, see eq. (2.4).

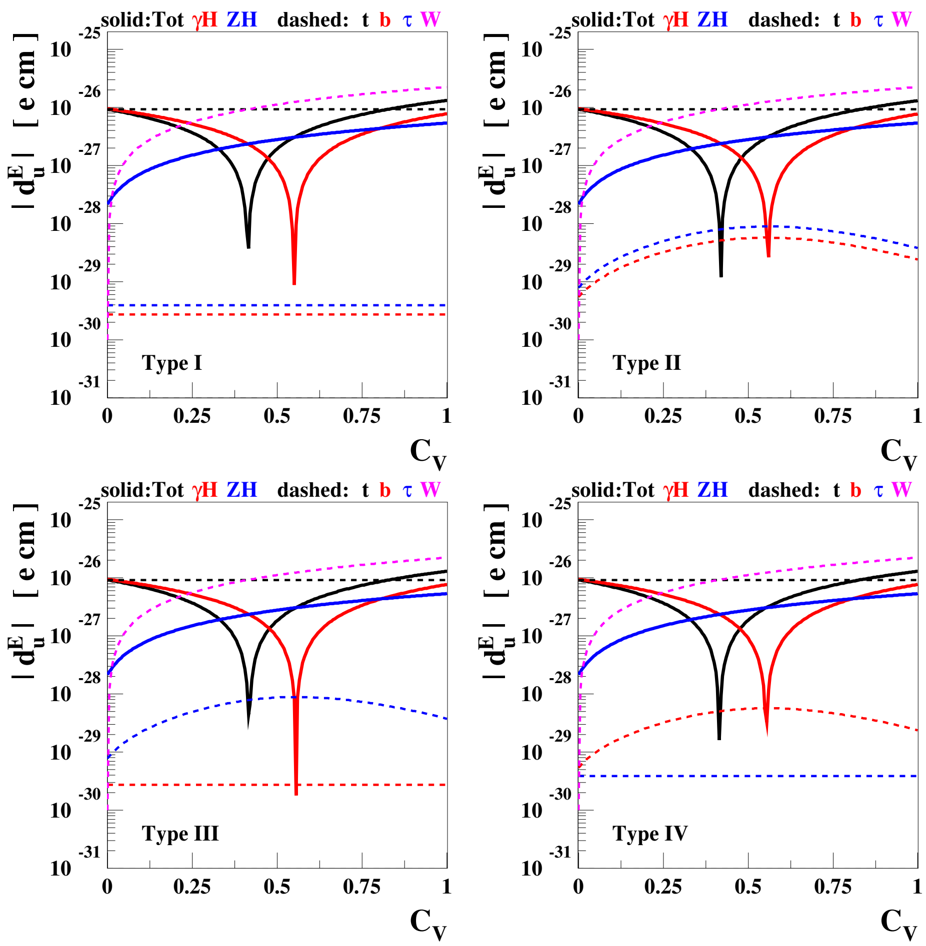

Figure 4. The same as in figure 2 but for the up-quark EDM.

the same as in figure 2. We find that the contributions from the Z-H Barr-Zee (solid blue lines) diagrams are comparable to those from the γ-H Barr-Zee (solid red lines) ones, and the Z-H Barr-Zee contributions are dominated by the W-boson loops. In this case, similar to the electron EDM case, the up-quark EDM satisfies

$$\left(\frac{d_u^E}{e}\right)_{\rm I,II,III,IV} \propto \left\{\left[\frac{16}{3}\left(f(\tau_{tH})+g(\tau_{tH})\right) C_u^S - C_v\, \mathcal{J}_W^\gamma(M_H)\right]\times\left(-\frac{2}{3}\right)+\frac{v_{Z\bar{u}u}}{s_W^2}\, C_v\, \mathcal{J}_W^Z(M_H)\right\} C_u^P \tag{4.5}$$

which are independent of the 2HDM type. We find $\mathcal{J}_W^Z(M_H) \simeq 5.5$. The top-quark contribution is negative and the W-loop contribution is positive because $v_{Z\bar{u}u} > 0$. One may see $(d_u^E)^{\gamma H}$ vanishes when the first two terms cancel and a cancellation may also occur between $(d_u^E)^{\gamma H}$ and $(d_u^E)^{ZH}$. The former cancellation explains the dips of $|(d_u^E)^{\gamma H}|$ (red solid lines) around $C_v = 0.55$ and the latter one explains the dips of the total (black solid lines) up-quark EDMs around $C_v = 0.4$

In figure 5, we show the absolute values of the down-quark EDM as a function of C_v in units of $e\,$cm with $C_u^S = C_u^P = 1/2$ for the Types I–IV of 2HDMs. The labeling of lines

JHEP06(2014)149

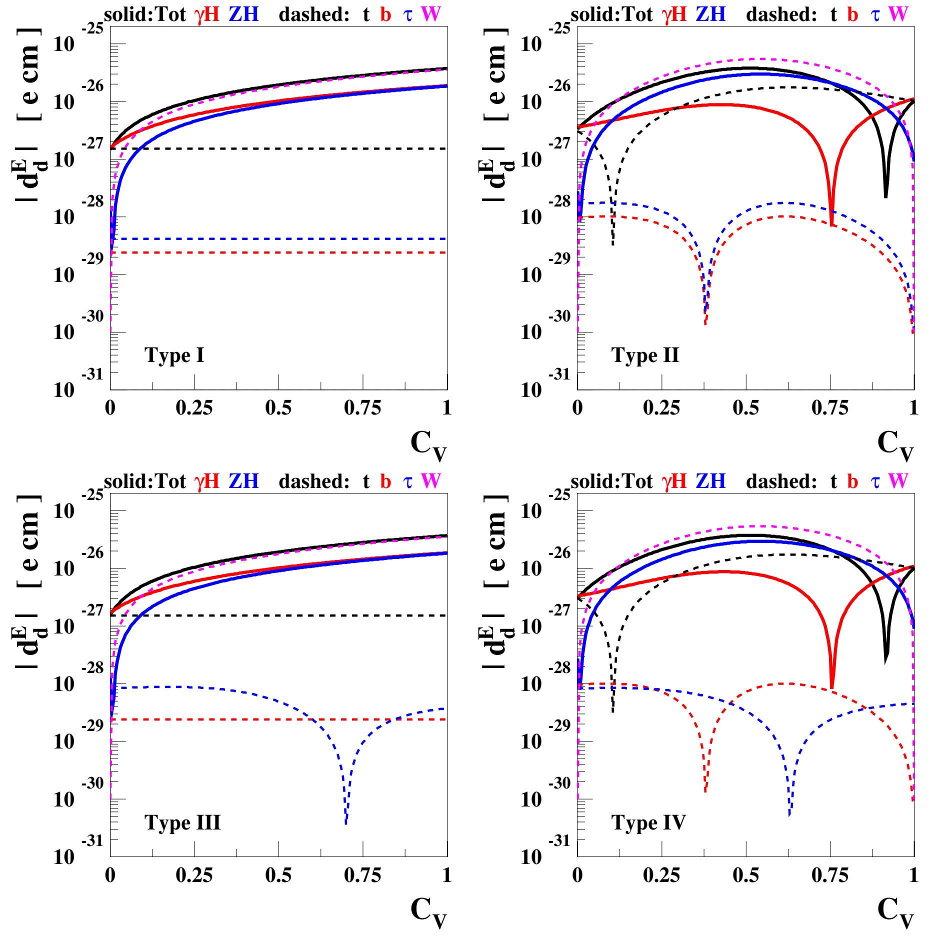

Figure 5. The same as in figure 2 but for the down-quark EDM.

is the same as in figure 2. Similar to the up-quark EDM, the γ-H Barr-Zee diagram is dominated by the top and W loops and the Z-H one by the W loop. Considering these three dominant constituent contributions, the down-quark EDM satisfies

$$\left(\frac{d_d^E}{e}\right)_{\rm I,III} \propto \left\{\left[\frac{16}{3}\left(-f(\tau_{tH})+g(\tau_{tH})\right)C_u^S + C_v\,\mathcal{J}_W^\gamma(M_H)\right]\times\left(\frac{1}{3}\right) - \frac{v_{Z\bar{d}d}}{s_W^2}\,C_v\,\mathcal{J}_W^Z(M_H)\right\}C_u^P,$$

$$\left(\frac{d_d^E}{e}\right)_{\rm II,IV} \propto \left\{\left[\frac{16}{3}\left(t_\beta^2 C_u^S\,f(\tau_{tH}) + \frac{O_{\phi_1 i}}{c_\beta}\,g(\tau_{tH})\right) - t_\beta^2 C_v\,\mathcal{J}_W^\gamma(M_H)\right]\times\left(\frac{1}{3}\right) + \frac{v_{Z\bar{d}d}}{s_W^2}\,t_\beta^2 C_v\,\mathcal{J}_W^Z(M_H)\right\}C_u^P. \tag{4.6}$$

First we note that all three contributions in Types I and III are positive because $v_{Z\bar{d}d} < 0$. As in the electron EDM, we find the top-quark contributions are independent of C_v. In Types II and IV, the two top-quark contributions cancel each other around $C_v = 0.1$ (dips of the black dashed lines) and they turn to be positive when $C_v \gtrsim 0.1$. Since both of the W loop contributions are negative, the cancellation between the positive top and negative W contributions explains the dips of $|(d_d^E)^{\gamma H}|$ around $C_v = 0.75$ (solid red lines) and those of the total sum (black solid lines) around $C_v = 0.9$. Note $t_\beta^2 C_v$ decreases as C_v increases when $C_v \gtrsim 0.5$.

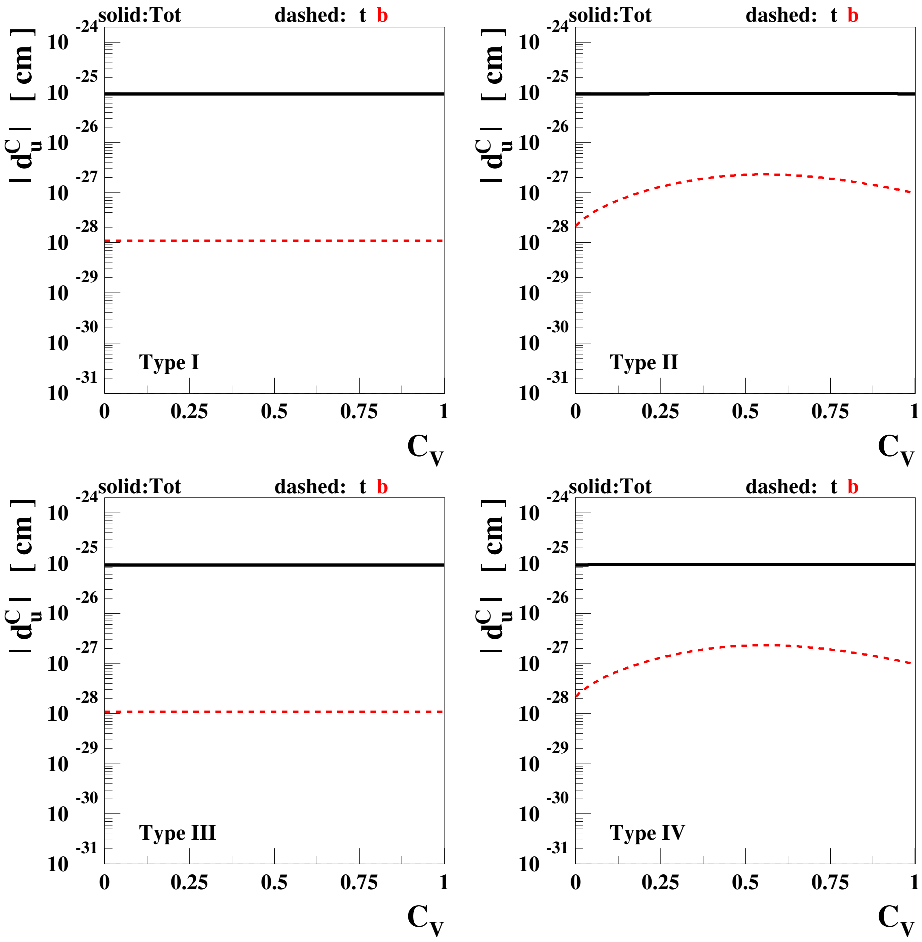

Figure 6. The absolute values of the up-quark CEDM as functions of C_v in units of cm when $C_u^S = C_u^P = 1/2$ for the types I–IV of 2HDMs. The constituent contributions from top and bottom loops are denoted by the dashed black and red lines, respectively, and the black solid lines are for the total sum.

In figure 6, we show the absolute values of the up-quark CEDM as a function of C_v in units of cm with $C_u^S = C_u^P = 1/2$ for Types I–IV of 2HDMs. The dashed black and red lines are for the top- and bottom-loop contributions, and the black solid line for the total sum. Since the Barr-Zee diagrams contributing to the up-quark CEDM are dominated by the top-quark loops, the black dashed lines almost overlap with black solid lines. Note that the top contributions are proportional to

$$(d_u^C)_{\mathrm{I,II,III,IV}} \propto -[f(\tau_{tH}) + g(\tau_{tH})]\, C_u^S\, C_u^P\,, \tag{4.7}$$

independent of the 2HDM types and of C_v: see eq. (3.11).

In figure 7, we show the absolute values of the down-quark CEDM as a function of C_v in units of cm with $C_u^S = C_u^P = 1/2$ for Types I–IV of 2HDMs. The labeling of lines is the

JHEP06(2014)149

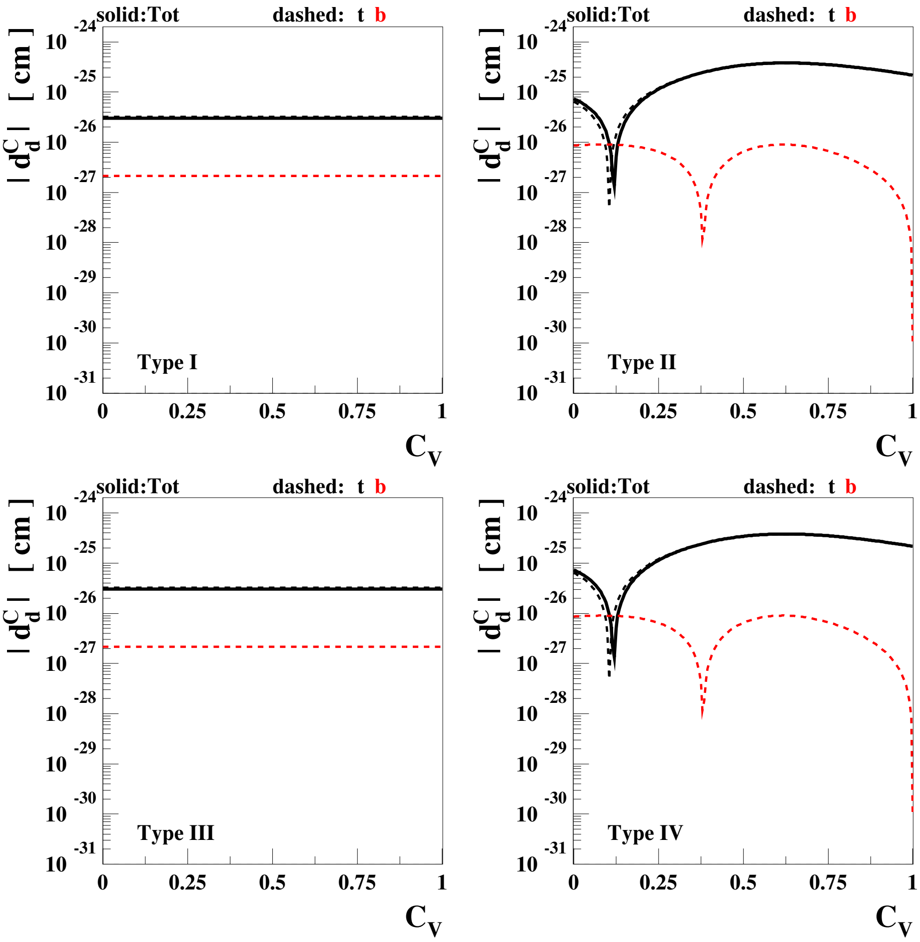

Figure 7. The same as in figure 6 but for the down-quark CEDM.

same as in figure 6. The dominant top-quark loop contributions are proportional to

$$(d_d^C)_{\rm I,III} \propto -[-f(\tau_{tH}) + g(\tau_{tH})]\, C_u^S\, C_u^P\,,$$
$$(d_d^C)_{\rm II,IV} \propto -\left[t_\beta^2 C_u^S\, f(\tau_{tH}) + \frac{O_{\phi_1 i}}{c_\beta}\, g(\tau_{tH})\right] C_u^P \tag{4.8}$$

for Types I, III and II, IV, respectively: see eq. (3.11). Therefore, in Types I and III, the top contributions are independent of C_v, while in Types II and IV there is cancellation around $C_v = 0.1$, similar to the top-quark contributions to d_d^E: see figure 5.

In figure 8, we show the absolute value of the coefficient of the Weinberg operator as a function of C_v in units of cm/MeV with $C_u^S = C_u^P = 1/2$ for Types I–IV of 2HDMs. The labeling of lines is the same as in figure 6. Again, the dominant contributions are from top loops which are proportional to

$$(d^G)_{\rm I,II,III,IV} \propto C_u^S\, C_u^P \tag{4.9}$$

and, accordingly, they are independent of C_v.

JHEP06(2014)149

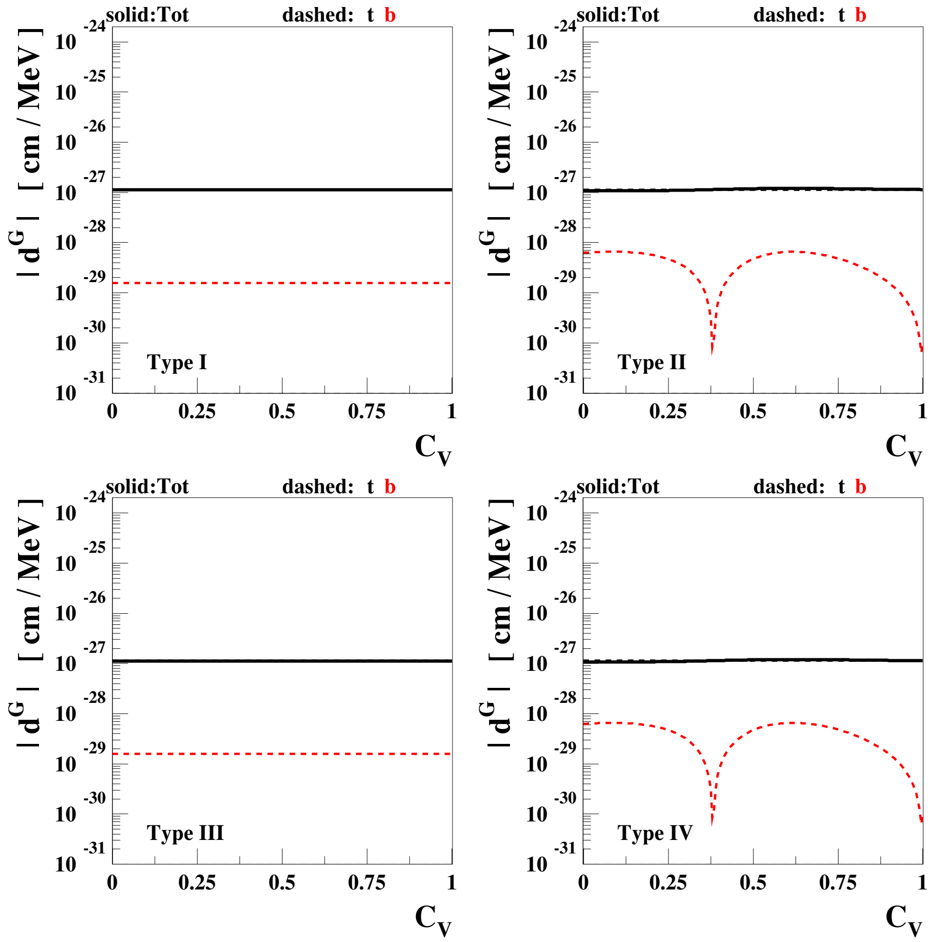

Figure 8. The same as in figure 6 but for the coefficient of the Weinberg operator in units of cm/MeV.

Before closing this subsection, we offer the following comments on the sizes of (C)EDMs of the light quarks and electron, and d^G.

- $|d_e^E| \sim 10^{-27}$–$10^{-26}\, e\,\text{cm}$ may induce $|d_{\text{Tl}}|/d_{\text{Tl}}^{\text{EXP}} \sim 1$, $|d_{\text{ThO}}/\mathcal{F}_{\text{ThO}}|/d_{\text{ThO}}^{\text{EXP}} \sim \mathcal{O}(10)$, and $|d_{\text{Hg}}|/d_{\text{Hg}}^{\text{EXP}} \sim \mathcal{O}(1)$: see eqs. (3.12), (3.15), and (3.19).
- $|d_u^E| \sim 10^{-26}\, e\,\text{cm}$ may induce $|d_{\text{n}}|/d_{\text{n}}^{\text{EXP}} \sim 10^{-1}$: see eq. (3.16).
- $|d_d^E| \sim 10^{-26}\, e\,\text{cm}$ may induce $|d_{\text{n}}|/d_{\text{n}}^{\text{EXP}} \sim 1$: see eq. (3.16).
- $|d_{u,d}^C| \sim 10^{-25}\,\text{cm}$ may induce $|d_{\text{n}}|/d_{\text{n}}^{\text{EXP}} \sim \mathcal{O}(1)$ and $|d_{\text{Hg}}^{\text{I}}|/d_{\text{Hg}}^{\text{EXP}} \sim \mathcal{O}(10)$: see eqs. (3.16) and (3.19).
- $|d^G| \sim 10^{-27}\,\text{cm/MeV}$ may induce $|d_{\text{n}}|/d_{\text{n}}^{\text{EXP}} \sim 6$: see eq. (3.16).

Therefore, the most significant constraints come from the thorium-monoxide EDM through d_e^E, Mercury EDM through $d_{u,d}^C$, and neutron EDM through d^G. We are going to present more details in the next subsection.

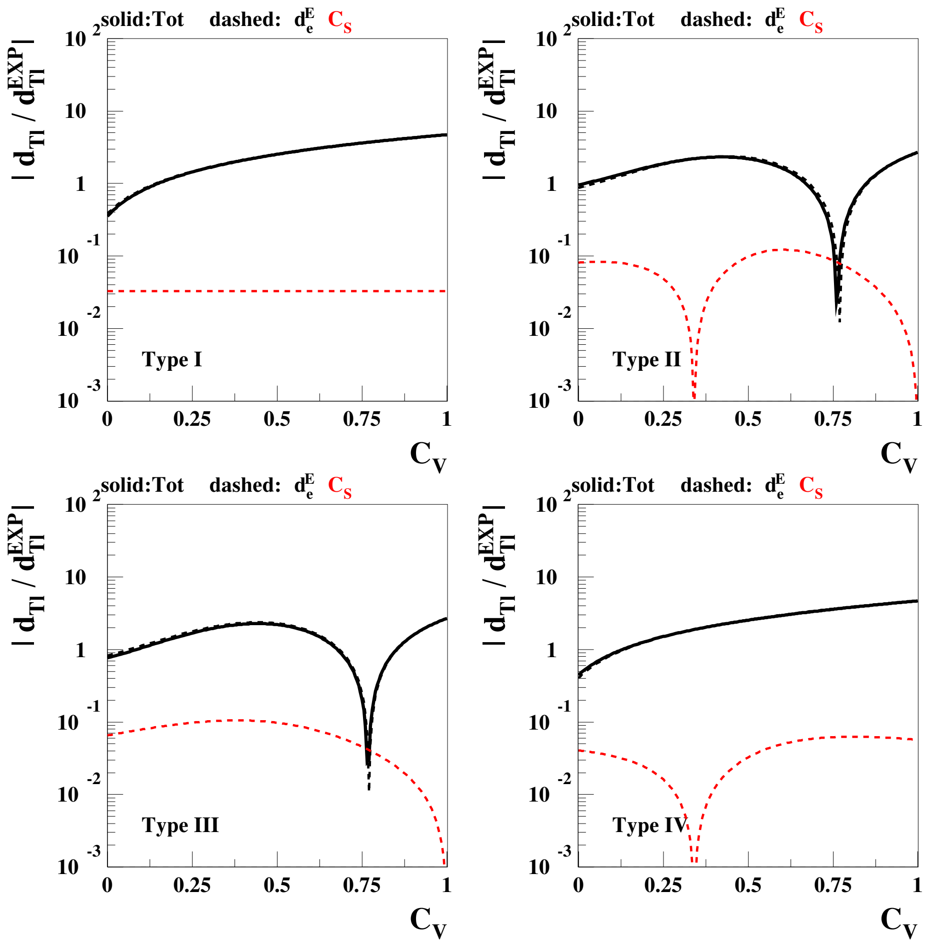

Figure 9. The absolute values of the Thallium EDM as functions of C_v divided by the current experimental limit $d_{\rm Tl}^{\rm EXP} = 9 \times 10^{-25}\, e\,{\rm cm}$ when $C_u^S = C_u^P = 1/2$ for the types I–IV of 2HDMs. The constituent contributions from d_e^E and C_S are denoted by the dashed black and red lines and the black solid lines are for the total sum.

4.2 Observable EDMs

In this subsection, we numerically analyze the Thallium, thorium-monoxide, neutron, and Mercury EDMs together with their constituent contributions, taking the benchmark point of $C_u^S = C_u^P = 1/2$.

In figure 9, we show the Thallium EDM normalized to the current experimental limit in eq. (4.2) as functions of C_v, and in figure 10 for the normalized thorium-monoxide EDM $d_{\rm ThO}/\mathcal{F}_{\rm ThO}$. Both of them are dominated by the electron EDM. With slightly different subleading C_S contributions, the behavior and parametric dependence of the two EDMs are almost the same: see eqs. (3.12) and (3.15), We observe that the thorium-monoxide EDM indeed provides one-order of magnitude stronger limits. We find $|(d_{\rm ThO}/\mathcal{F}_{\rm ThO})/d_{\rm ThO}^{\rm EXP}| \lesssim 100$ (I, IV) and $\lesssim 50$ (II, III). Moreover, because of the dips near $C_v = 0.75$ due to the cancellations between the top- and W-loop contributions to d_e^E in Types II and III, the thorium-monoxide EDM constraints are shown to be weaker in Types II and III. It is

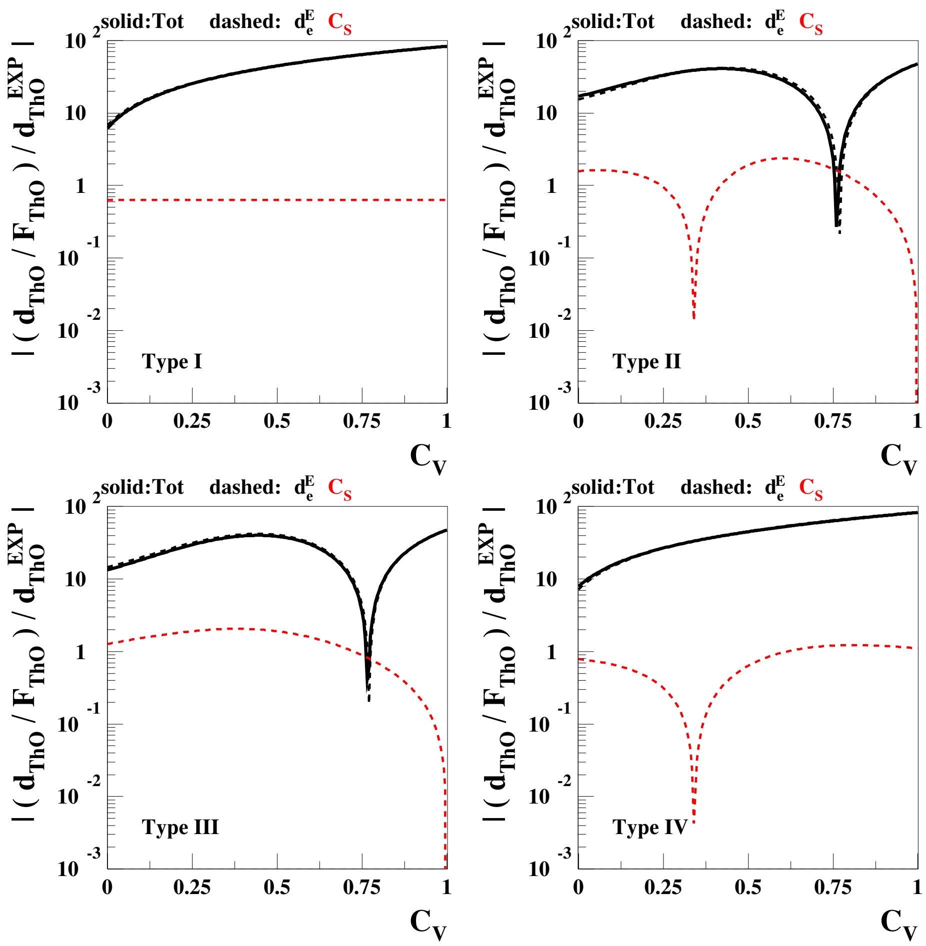

Figure 10. The same as in figure 9 but for the normalized thorium-monoxide EDM $d_{\rm ThO}/\mathcal{F}_{\rm ThO}$ with $d_{\rm ThO}^{\rm EXP} = 8.7 \times 10^{-29}\,e\,{\rm cm}$.

interesting to note that the thorium-monoxide EDM even shows a sensitivity to the C_S contribution.

Figure 11 shows the neutron EDM (black sold lines) and its constituent contributions from $d^E_{u,d}$, $d^C_{u,d}$, d^G, and the four-fermion operators as functions of C_v taking $C^S_u = C^P_u = 1/2$. We observe $|d_{\rm n}/d_{\rm n}^{\rm EXP}| \lesssim 10$. We also observe the $d^C_{u,d}$ (red dashed lines) and d^G (blue dashed lines) contributions dominate and they have opposite signs to each other except for the regions near $C_v = 0$ in Types II and IV. The cancellation between the $d^C_{u,d}$ and d^G contributions is most prominent at $C_v = 0.25$ in Types II and IV, but the milder cancellation around $C_v = 1$ is phenomenologically more important because the current Higgs data prefer the region around $C_v = 1$. The cancellation around $C_v = 1$ makes the neutron EDM constraints in Types II and IV weaker than in Types I and III, as shown in figure 11. We note that, in Types I and III the neutron EDM also show a sensitivity to the $d^E_{u,d}$ EDMs (black dashed lines) near $C_v = 1$.

Figure 12 shows the Mercury EDM (black sold lines) using $d^{\rm I}_{\rm Hg}[S]$ for the Schiff moment and its constituent contributions from the Schiff moment, d^E_e, C_S, and $C^{(\prime)}_P$ as functions of

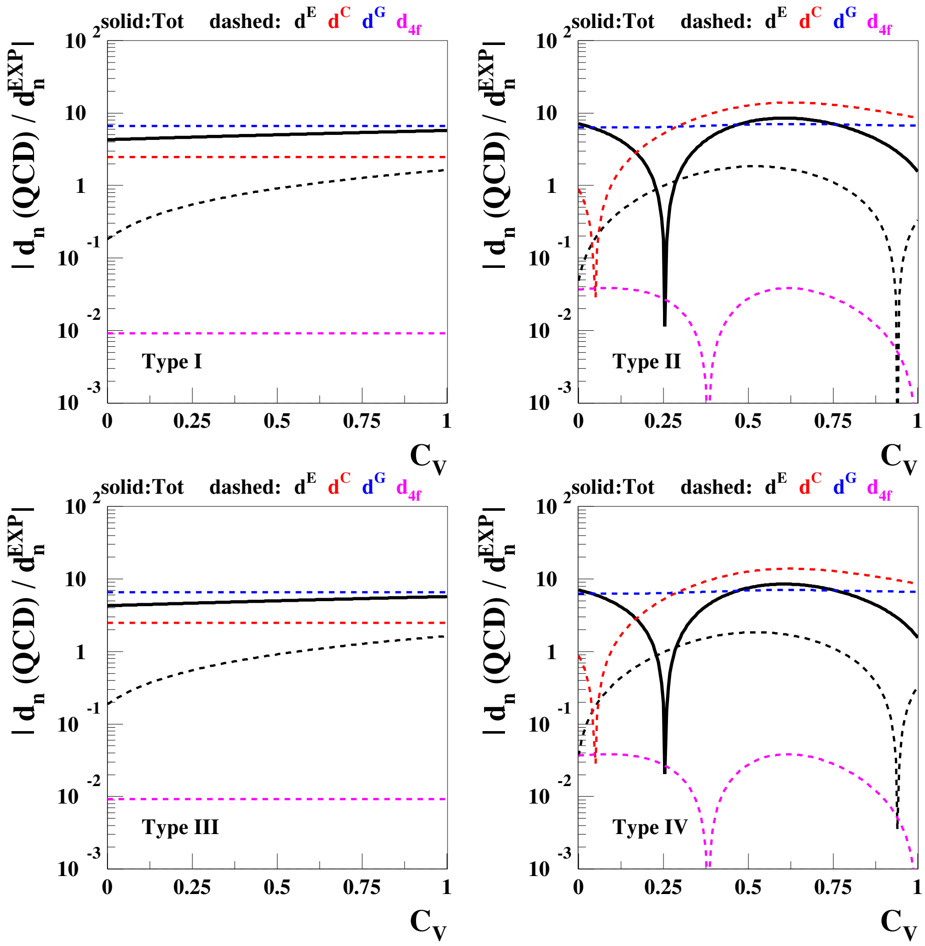

Figure 11. The absolute values of the neutron EDM in the QCD sum-rule approach as functions of C_v divided by the current experimental limit $d_{\rm n}^{\rm EXP} = 2.9 \times 10^{-26}\,e\,{\rm cm}$ when $C_u^S = C_u^P = 1/2$ for the types I–IV of 2HDMs. The constituent contributions from $d^E_{u,d}$, $d^C_{u,d}$, d^G, and the four-fermion operators (d_{4f}) are denoted by the dashed black, red, blue, and magenta lines. The black solid lines are for the total sum.

C_v taking $C_u^S = C_u^P = 1/2$. We observe $|d_{\rm Hg}/d_{\rm Hg}^{\rm EXP}| \approx 10$ (I, III) and 30 (II, IV) around $C_v = 1$. The Mercury EDM is dominated by the contributions from the Schiff moment (dashed black lines) and has also a sensitivity to the electron EDM (red dashed lines) near $C_v = 1$.

4.3 EDM constraints

In this subsection, we present the CL regions in the C_u^S–C_u^P plane which satisfy the current Higgs-boson data and various EDM constraints.

In figure 13, we show the allowed regions satisfying the Higgs-boson data and the thorium-monoxide EDM constraint at 68.3% (red), 95% (green), and 99.7% (blue) CL in the plane of C_u^S vs C_u^P for Types I–IV. We recall that the CL regions before applying the EDM constraints have been shown in figure 1. For each allowed point in the C_u^S–

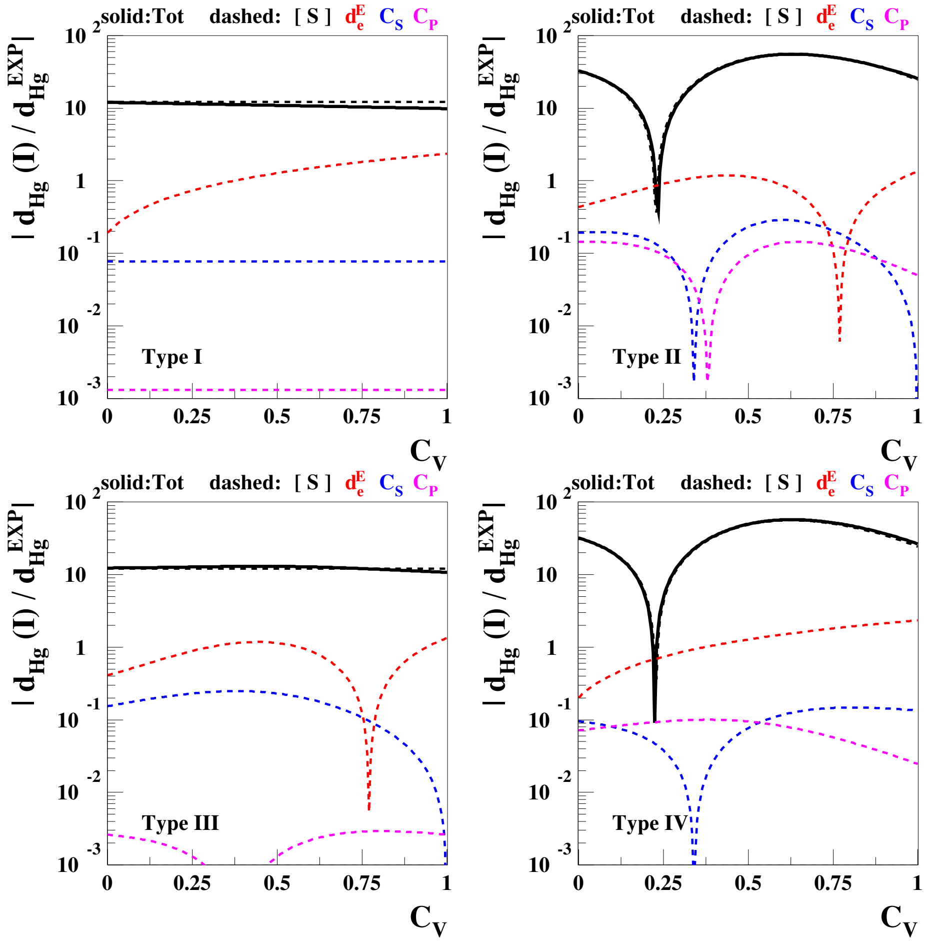

Figure 12. The absolute values of the Mercury EDM using $d^{\rm I}_{\rm Hg}[S]$ as functions of C_v divided by the current experimental limit $d^{\rm EXP}_{\rm Hg} = 3.1 \times 10^{-29}\, e\,{\rm cm}$ when $C_u^S = C_u^P = 1/2$ for Types I–IV of 2HDMs. The constituent contributions from the Schiff moment, d_e^E, C_S, and $C_P^{(\prime)}$ are denoted by the dashed black, red, blue, and magenta lines. The black solid lines are for the total sum.

C_u^P plane in figure 1, the thorium-monoxide EDM is calculated, and we accept the point if $|(d_{\rm ThO}/\mathcal{F}_{\rm ThO})/d^{\rm EXP}_{\rm ThO}| \leq 1$ is satisfied while varying C_v within the corresponding CL regions.[4] We observe that $C_u^P \neq 0$ is strongly constrained in Types I and IV. While in Types II and III, the constraints are weaker in the regions centered around the point $C_u^S = 1$ due to the cancellation between the top- and W-loop contributions to the dominant electron EDM: see figures 2 and 10. We find that $|C_u^P|$ can be as large as ~ 0.6 for Types II and III at 95% CL (green regions).

Figure 14 shows the allowed regions satisfying the Higgs-boson data and the neutron EDM constraint at 68.3% (red), 95% (green), and 99.7% (blue) CL, respectively, in the plane of C_u^S vs C_u^P for Type I–IV. The allowed regions are obtained in the same way as in the case of thorium-monoxide. The neutron EDM constraint is weaker in Types II and IV

[4] We are not showing the Thallium EDM constraints since they are always weaker than those from the thorium-monoxide EDM.

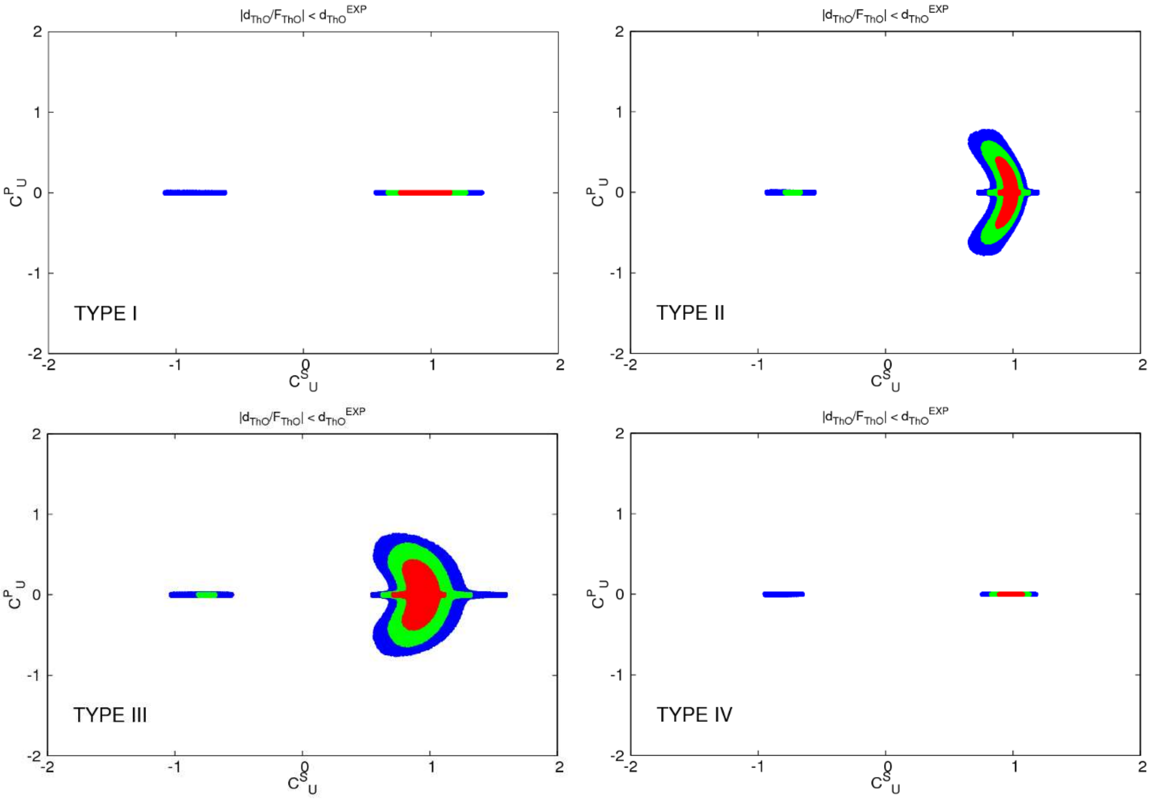

Figure 13. The same as in figure 1 but with the thorium-monoxide EDM constraint $|(d_{\rm ThO}/\mathcal{F}_{\rm ThO})/d_{\rm ThO}^{\rm EXP}| \leq 1$ applied.

due to the cancellation between the $d^C_{u,d}$ and d^G contributions around $C_v = 1$: see figure 11. We find that $|C_u^P|$ can be as large as ~ 0.6 for Types II and IV at 95% CL (green regions).

Figure 15 is the same as in figures 13 and 14 but with the Mercury EDM constraint applied. In contrast to the weaker thorium-monoxide (neutron) EDM constraint in Types II and III (Types II and IV), the Mercury EDM constraint is almost equally stringent in all four types and, specifically, $|C_u^P|$ is restricted to be ~ 0.1 for Types II and IV.

The combined constraint at 95% CL from all the EDMs measurements and the Higgs-boson data is obtained in figure 16. The black regions in figure 16 shows the 95% CL regions satisfying the Thallium, thorium-monoxide, neutron, and Mercury EDM constraints simultaneously, as well as the Higgs-boson data. We find that the combination of all available EDM experiments provide remarkably tight bounds on CP violation. Thus, non-zero values of C_u^P are stringently restricted as

$$|C_u^P| \lesssim 7\times 10^{-3}\ ({\rm I})\,, \qquad 2\times 10^{-2}\ ({\rm II})\,, \qquad 3\times 10^{-2}\ ({\rm III})\,, \qquad 6\times 10^{-3}\ ({\rm IV})\,. \tag{4.10}$$

Since we have only taken into account the 125.5 GeV Higgs-mediated EDMs, there could possibly be other contributions to the EDMs if the 125.5 GeV Higgs H is embedded in the models beyond the SM. The additional contributions are model dependent and, for example, they are induced by the other Higgs bosons in the 2HDM framework, from some supersymmetric particles in SUSY models, etc. One may expect that cancellations may

JHEP06(2014)149

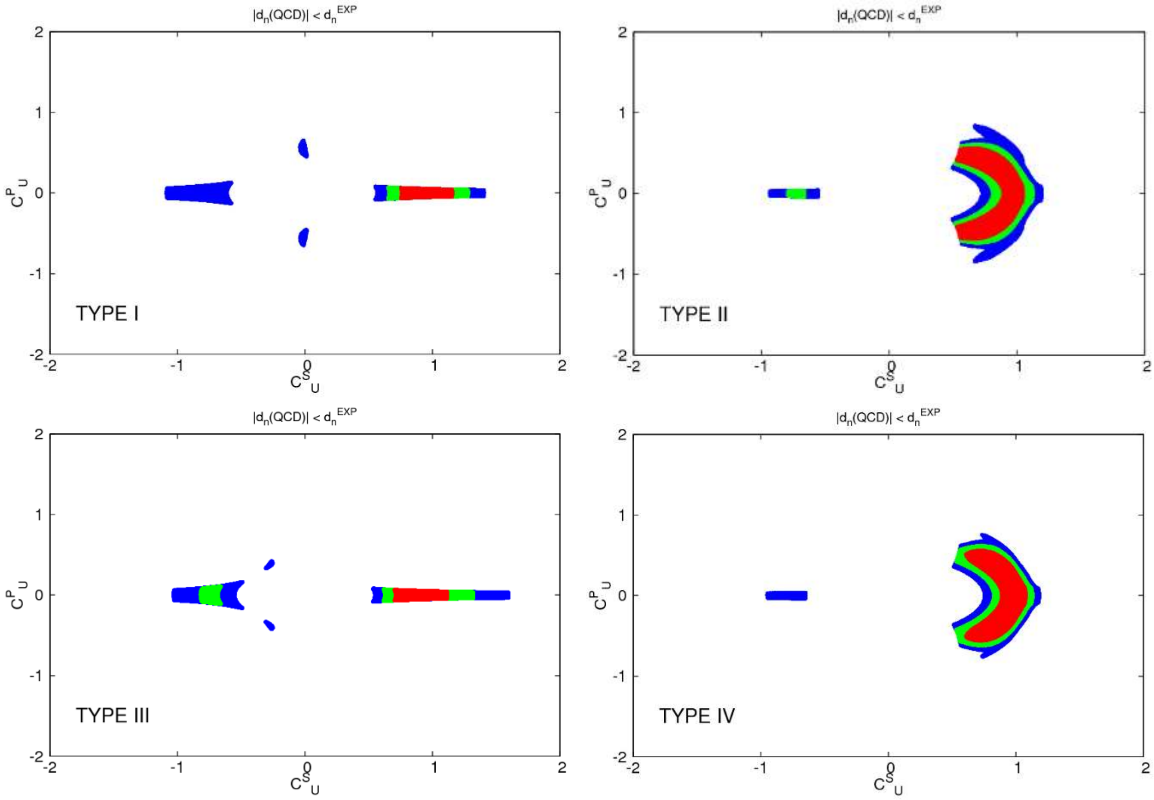

Figure 14. The same as in figure 1 but with the neutron EDM constraint constraint $|d_{\rm n}/d_{\rm n}^{\rm EXP}| \leq 1$ applied.

occur between the H-mediated and these additional contributions. In this case, the EDM constraints can be relaxed. In figure 16, we also show the 95% CL regions satisfying the relaxed constraints

$$|d_{\rm Tl,n,Hg}/d_{\rm Tl,n,Hg}^{\rm EXP}| \leq r \qquad \text{and} \qquad |(d_{\rm ThO}/\mathcal{F}_{\rm ThO})/d_{\rm ThO}^{\rm EXP}| \leq r \tag{4.11}$$

with the relaxation factor $r = 10$ (orange), 30 (pink), and 100 (green). The factor r, say $r = 100$, represents a fine-tuning of order 10^{-2}. If the degree of cancellation is 90% (99%), with 100% corresponding to a complete cancellation, the orange (green) regions with $r = 10\,(100)$ are allowed. For $r = 10$, $|C_u^P|$ can be as large as ~ 0.1 (I), ~ 0.2 (II), ~ 0.4 (III), and ~ 0.1 (IV). When $r = 100$, we observe the whole 95% CL regions are allowed in Types I, II, and IV. In Type III, the whole 95% CL region is allowed for the smaller $r = 30$.

Finally, in figure 17, we show the correlation between $|d_{\rm D}/d_{\rm D}^{\rm PRJ}|$ and $|d_{\rm Ra}/d_{\rm Ra}^{\rm PRJ}|$ in the colored regions of figure 16 with $r = 1$ (black), $r = 10$ (orange), 30 (pink), and 100 (green). Note that the projected sensitivities for the deuteron EDM $d_D^{\rm PRJ}$ and the Radium EDM $d_{Ra}^{\rm PRJ}$ can be found right after eq. (4.2). The strong correlations seen in Types I and III can be understood by observing that the dominant contributions to $d_{\rm D}$ and $d_{\rm Ra}$ coming from $d_{u,d}^C$ and d^G are all proportional to the product $C_u^S \times C_u^P$ with no dependence on C_v, see figures 6, 7, and 8. The ratios $|d_{\rm D}/d_{\rm D}^{\rm PRJ}|$ and $|d_{\rm Ra}/d_{\rm Ra}^{\rm PRJ}|$ lying in the ranges from about

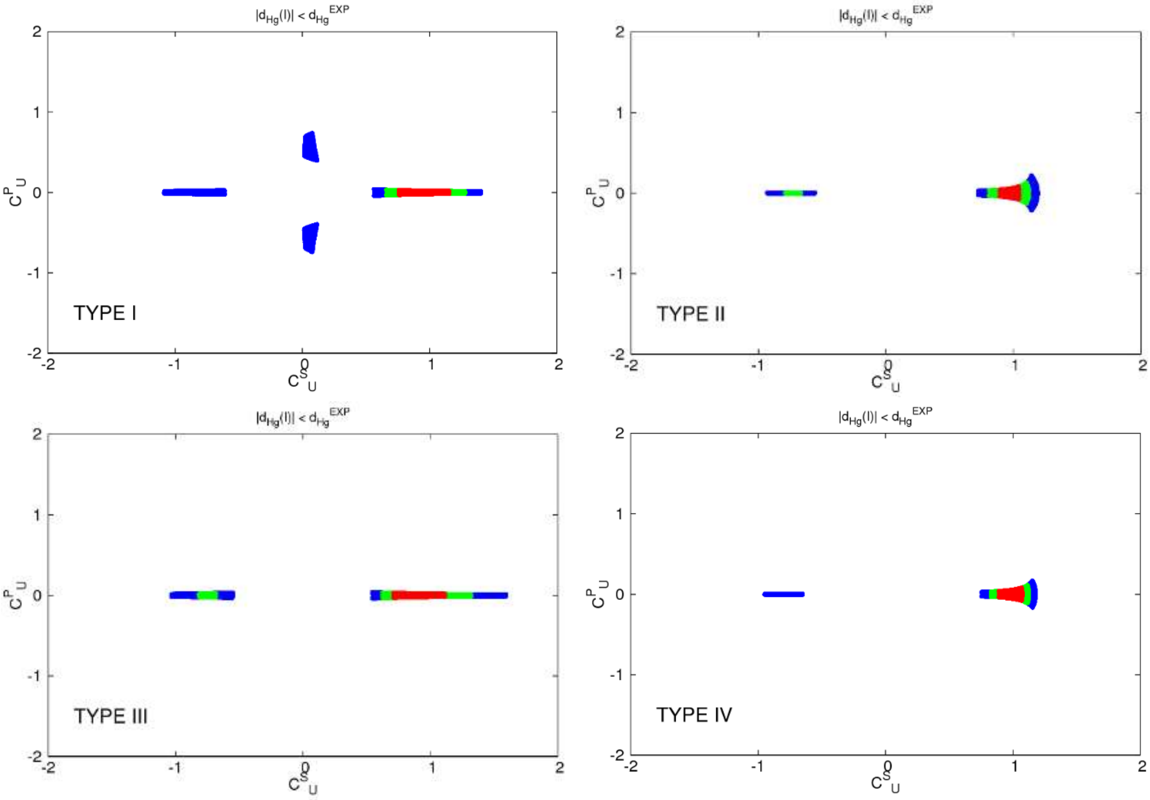

Figure 15. The same as in figure 1 but with the Mercury EDM constraint $|d^{\mathrm{I}}_{\mathrm{Hg}}/d^{\mathrm{EXP}}_{\mathrm{Hg}}| \leq 1$ applied.

10 and 100 require the degree of cancellation of 90% (orange regions). Even in the black regions ($r = 1$) without any additional contributions beyond those from the 125.5 GeV Higgs, we find that the deuteron EDM can be 5 (I), 10 (II), 15 (III), and 8 (IV) times as large as the projected experimental sensitivity. While those for the Radium EDM are 2 (I), 7 (II), 6 (III), and 7 (IV) times as large as the experimental sensitivity. It means that the deuteron and Radium EDMs can be easily above the projected sensitivities offered by the new experiments even when the combined EDM constraints are the most stringent without assuming any additional contributions beyond those from the 125.5 GeV Higgs boson.

5 Conclusions

In this work, we have updated the Higgcision constraints on the Higgs boson couplings to SM gauge bosons and fermions, and confronted the allowed parameter space in C_u^S, C_u^P, and C_v against various EDM constraints from the non-observation of the Thallium (^{205}Tl), thorium-monoxide (ThO), neutron, and Mercury (^{199}Hg) EDMs, in the framework of 2HDMs. Although the Higgs boson data still allow sizable C_u^P, the combined EDM constraints restrict $|C_u^P|$ to a very small value of $\sim 10^{-2}$.

We have only considered the contributions from the 125.5 GeV Higgs boson via the Higgs-mediated diagrams in this work. There could potentially be contributions from other particles of any new physics models, e.g., the heavier Higgs bosons of multi-Higgs models,

JHEP06(2014)149

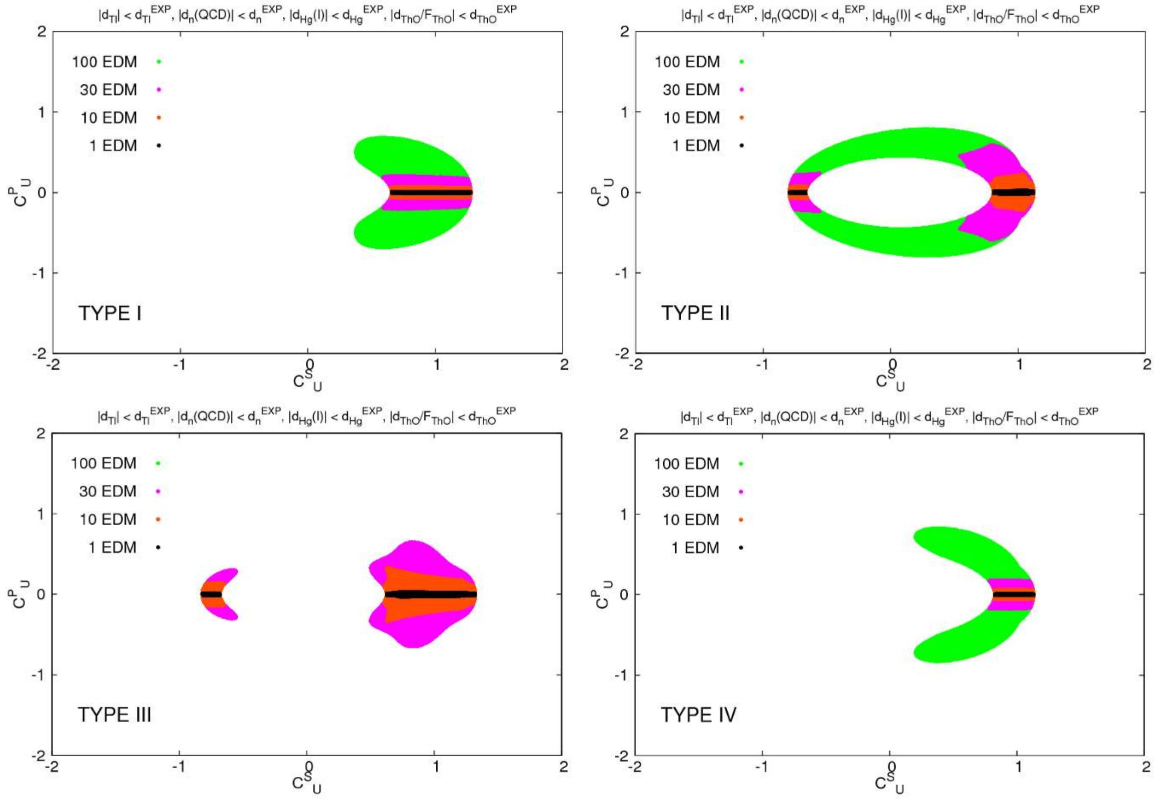

Figure 16. The 95% CL regions satisfying the Thallium, thorium-monoxide, neutron, and Mercury EDM constraints (black) simultaneously, as well as the Higgs data. The orange, pink, and green regions are for the cases of applying relaxed constraints $|d_{\rm Tl,n,Hg}/d^{\rm EXP}_{\rm Tl,n,Hg}| \leq r$ and $|(d_{\rm ThO}/\mathcal{F}_{\rm ThO})/d^{\rm EXP}_{\rm ThO}| \leq r$ with the relaxation factor $r = 10$ (orange), 30 (pink), and 100 (green).

supersymmetric particles, or any other exotic particles that carry CP-violating couplings. These contributions and the contributions from the 125.5 GeV Higgs boson could cancel each other in a delicate way. If we allow 1% fine tuning, the constraints on the pseudoscalar coupling C_u^P are relaxed and $|C_u^P|$ as large as 0.5 can be allowed.

In the following we offer a few more comments before we close.

1. The observable EDMs involve the electron EDM d_e^E, (C)EDMs of the up and down quarks $d_{u,d}^{E,C}$, and the coefficient of the Weinberg operator d^G. Only d^G is independent of the Higgs couplings to the first-generation fermions.

2. The observed 125.5 Higgs boson, which is denoted as H in this work, gives definite predictions for d_e^E and $d_{u,d}^{E,C}$ through the two-loop Barr-Zee diagrams.

3. For d_e^E, we consider both the Barr-Zee diagrams mediated by the γ-γ-H couplings and by the γ-H-Z couplings with the constituent contributions from top, bottom, tau, and W-boson loops. We note the γ-γ-H Barr-Zee diagrams are dominant. We further observe that the contributions from top and W-boson loops are dominant and a cancellation occurs between them around $C_v = 1$ in Types II and III. Note the current Higgs data prefer the region around $C_v = 1$.

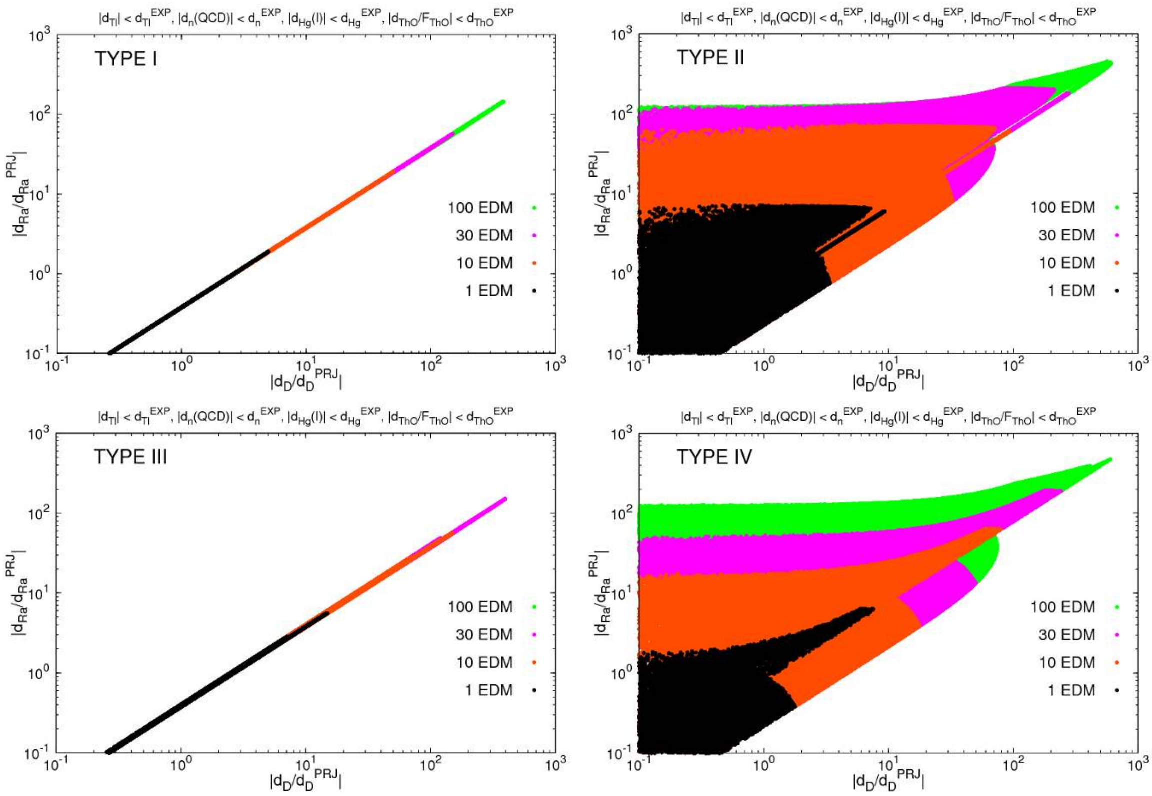

Figure 17. The correlation between $|d_{\rm D}/d_{\rm D}^{\rm PRJ}|$ and $|d_{\rm Ra}/d_{\rm Ra}^{\rm PRJ}|$ in the 95% CL regions satisfying the Thallium, thorium-monoxide, neutron, and Mercury EDM constraints simultaneously taking the relaxation factor $r = 1$ (black), $r = 10$ (orange), 30 (pink), and 100 (green).

4. For $d_{u,d}^E$, the contribution from the γ-γ-H and γ-H-Z Barr-Zee diagrams are comparable. In d_d^E, a cancellation occurs between them around $C_v = 1$ in Types II and IV.

5. The Barr-Zee contributions to $d_{u,d}^C$ are dominated by the top loops which are independent of the 2HDM types except for d_d^C in Types II and IV.

6. The dominant contributions to d^G from top loops are independent of the 2HDM types.

7. The Thallium and ThO EDMs are dominated by d_e^E, the neutron EDM by $d_{u,d}^C$ and d^G, and the Mercury EDM by $d_{u,d}^C$ through the Schiff moment. We observe a cancellation occurs between the contributions from $d_{u,d}^C$ and d^G to the neutron EDM around $C_v = 1$ in Types II and IV.

8. The ThO (neutron) EDM constraint is relatively weaker in Types II and III (Types II and IV), while the Mercury EDM constraint is almost equally stringent in all four types.

9. We find that the deuteron and Radium EDMs can be ~ 10 times as large as the projected experimental sensitivities even when $|C_u^P|$ is restricted to be smaller than about 10^{-2} by the combined EDM constraints.

Note added. After the completion of this work, we received a paper [105], which addresses the LHC Higgs and EDM constraints in Types I and II 2HDMs.

Acknowledgments

We thank Wouter Dekens and Jordy de Vries for helpful discussions and valuable comments. This work was supported the National Science Council of Taiwan under Grants No. 102-2112-M-007-015-MY3. J.S.L. was supported by the National Research Foundation of Korea (NRF) grant (No. 2013R1A2A2A01015406). This study was also financially supported by Chonnam National University, 2012.

References

[1] ATLAS collaboration, *Observation of a new particle in the search for the standard model Higgs boson with the ATLAS detector at the LHC*, *Phys. Lett.* **B 716** (2012) 1 [arXiv:1207.7214] [INSPIRE].

[2] CMS collaboration, *Observation of a new boson at a mass of 125 GeV with the CMS experiment at the LHC*, *Phys. Lett.* **B 716** (2012) 30 [arXiv:1207.7235] [INSPIRE].

[3] D. Carmi, A. Falkowski, E. Kuflik and T. Volansky, *Interpreting LHC Higgs results from natural new physics perspective*, *JHEP* **07** (2012) 136 [arXiv:1202.3144] [INSPIRE].

[4] A. Azatov, R. Contino and J. Galloway, *Model-independent bounds on a light Higgs*, *JHEP* **04** (2012) 127 [*Erratum ibid.* **04** (2013) 140] [arXiv:1202.3415] [INSPIRE].

[5] J.R. Espinosa, C. Grojean, M. Muhlleitner and M. Trott, *Fingerprinting Higgs suspects at the LHC*, *JHEP* **05** (2012) 097 [arXiv:1202.3697] [INSPIRE].

[6] M. Klute, R. Lafaye, T. Plehn, M. Rauch and D. Zerwas, *Measuring Higgs couplings from LHC data*, *Phys. Rev. Lett.* **109** (2012) 101801 [arXiv:1205.2699] [INSPIRE].

[7] D. Carmi, A. Falkowski, E. Kuflik and T. Volansky, *Interpreting the 125 GeV Higgs*, *Nuovo Cim.* **C 035** (2012) 315 [arXiv:1206.4201] [INSPIRE].

[8] I. Low, J. Lykken and G. Shaughnessy, *Have we observed the Higgs (imposter)?*, *Phys. Rev.* **D 86** (2012) 093012 [arXiv:1207.1093] [INSPIRE].

[9] P.P. Giardino, K. Kannike, M. Raidal and A. Strumia, *Is the resonance at 125 GeV the Higgs boson?*, *Phys. Lett.* **B 718** (2012) 469 [arXiv:1207.1347] [INSPIRE].

[10] J. Ellis and T. You, *Global analysis of the Higgs candidate with mass* ~ 125 *GeV*, *JHEP* **09** (2012) 123 [arXiv:1207.1693] [INSPIRE].

[11] J.R. Espinosa, C. Grojean, M. Muhlleitner and M. Trott, *First glimpses at Higgs' face*, *JHEP* **12** (2012) 045 [arXiv:1207.1717] [INSPIRE].

[12] D. Carmi, A. Falkowski, E. Kuflik, T. Volansky and J. Zupan, *Higgs after the discovery: a status report*, *JHEP* **10** (2012) 196 [arXiv:1207.1718] [INSPIRE].

[13] S. Banerjee, S. Mukhopadhyay and B. Mukhopadhyaya, *New Higgs interactions and recent data from the LHC and the Tevatron*, *JHEP* **10** (2012) 062 [arXiv:1207.3588] [INSPIRE].

[14] F. Bonnet, T. Ota, M. Rauch and W. Winter, *Interpretation of precision tests in the Higgs sector in terms of physics beyond the standard model*, *Phys. Rev.* **D 86** (2012) 093014 [arXiv:1207.4599] [INSPIRE].

[15] T. Plehn and M. Rauch, *Higgs couplings after the discovery*, *Europhys. Lett.* **100** (2012) 11002 [arXiv:1207.6108] [INSPIRE].

[16] A. Djouadi, *Precision Higgs coupling measurements at the LHC through ratios of production cross sections*, *Eur. Phys. J.* **C 73** (2013) 2498 [arXiv:1208.3436] [INSPIRE].

[17] B.A. Dobrescu and J.D. Lykken, *Coupling spans of the Higgs-like boson*, *JHEP* **02** (2013) 073 [arXiv:1210.3342] [INSPIRE].

[18] G. Cacciapaglia, A. Deandrea, G.D. La Rochelle and J.-B. Flament, *Higgs couplings beyond the standard model*, *JHEP* **03** (2013) 029 [arXiv:1210.8120] [INSPIRE].

[19] A. Freitas and P. Schwaller, *Higgs CP properties from early LHC data*, *Phys. Rev.* **D 87** (2013) 055014 [arXiv:1211.1980] [INSPIRE].

[20] G. Bélanger, B. Dumont, U. Ellwanger, J.F. Gunion and S. Kraml, *Higgs couplings at the end of 2012*, *JHEP* **02** (2013) 053 [arXiv:1212.5244] [INSPIRE].

[21] G. Moreau, *Constraining extra-fermion(s) from the Higgs boson data*, *Phys. Rev.* **D 87** (2013) 015027 [arXiv:1210.3977] [INSPIRE].

[22] K. Cheung, J.S. Lee and P.-Y. Tseng, *Higgs precision (Higgcision) era begins*, *JHEP* **05** (2013) 134 [arXiv:1302.3794] [INSPIRE].

[23] P.P. Giardino, K. Kannike, I. Masina, M. Raidal and A. Strumia, *The universal Higgs fit*, *JHEP* **05** (2014) 046 [arXiv:1303.3570] [INSPIRE].

[24] P. Bechtle, S. Heinemeyer, O. Stål, T. Stefaniak and G. Weiglein, *HiggsSignals: confronting arbitrary Higgs sectors with measurements at the Tevatron and the LHC*, *Eur. Phys. J.* **C 74** (2014) 2711 [arXiv:1305.1933] [INSPIRE].

[25] A. Djouadi and G. Moreau, *The couplings of the Higgs boson and its CP properties from fits of the signal strengths and their ratios at the 7+8 TeV LHC*, *Eur. Phys. J.* **C 73** (2013) 2512 [arXiv:1303.6591] [INSPIRE].

[26] A. Falkowski, F. Riva and A. Urbano, *Higgs at last*, *JHEP* **11** (2013) 111 [arXiv:1303.1812] [INSPIRE].

[27] T. Corbett, O.J.P. Eboli, J. Gonzalez-Fraile and M.C. Gonzalez-Garcia, *Constraining anomalous Higgs interactions*, *Phys. Rev.* **D 86** (2012) 075013 [arXiv:1207.1344] [INSPIRE].

[28] T. Corbett, O.J.P. Eboli, J. Gonzalez-Fraile and M.C. Gonzalez-Garcia, *Robust determination of the Higgs couplings: power to the data*, *Phys. Rev.* **D 87** (2013) 015022 [arXiv:1211.4580] [INSPIRE].

[29] E. Masso and V. Sanz, *Limits on anomalous couplings of the Higgs to electroweak gauge bosons from LEP and LHC*, *Phys. Rev.* **D 87** (2013) 033001 [arXiv:1211.1320] [INSPIRE].

[30] E. Boos, V. Bunichev, M. Dubinin and Y. Kurihara, *Higgs boson signal at complete tree level in the SM extension by dimension-six operators*, *Phys. Rev.* **D 89** (2014) 035001 [arXiv:1309.5410] [INSPIRE].

[31] S. Banerjee, S. Mukhopadhyay and B. Mukhopadhyaya, *Higher dimensional operators and LHC Higgs data: the role of modified kinematics*, *Phys. Rev.* **D 89** (2014) 053010 [arXiv:1308.4860] [INSPIRE].

[32] J. Cao, P. Wan, J.M. Yang and J. Zhu, *The SM extension with color-octet scalars: diphoton enhancement and global fit of LHC Higgs data*, JHEP **08** (2013) 009 [arXiv:1303.2426] [INSPIRE].

[33] H.S. Cheon and S.K. Kang, *Constraining parameter space in type-II two-Higgs doublet model in light of a 126 GeV Higgs boson*, JHEP **09** (2013) 085 [arXiv:1207.1083] [INSPIRE].

[34] N. Craig and S. Thomas, *Exclusive signals of an extended Higgs sector*, JHEP **11** (2012) 083 [arXiv:1207.4835] [INSPIRE].

[35] D.S.M. Alves, P.J. Fox and N.J. Weiner, *Higgs signals in a type I 2HDM or with a sister Higgs*, arXiv:1207.5499 [INSPIRE].

[36] W. Altmannshofer, S. Gori and G.D. Kribs, *A minimal flavor violating 2HDM at the LHC*, Phys. Rev. **D 86** (2012) 115009 [arXiv:1210.2465] [INSPIRE].

[37] S. Chang et al., *Comprehensive study of two Higgs doublet model in light of the new boson with mass around 125 GeV*, JHEP **05** (2013) 075 [arXiv:1210.3439] [INSPIRE].

[38] Y. Bai, V. Barger, L.L. Everett and G. Shaughnessy, *General two Higgs doublet model (2HDM-G) and Large Hadron Collider data*, Phys. Rev. **D 87** (2013) 115013 [arXiv:1210.4922] [INSPIRE].

[39] A. Drozd, B. Grzadkowski, J.F. Gunion and Y. Jiang, *Two-Higgs-doublet models and enhanced rates for a 125 GeV Higgs*, JHEP **05** (2013) 072 [arXiv:1211.3580] [INSPIRE].

[40] A. Celis, V. Ilisie and A. Pich, *LHC constraints on two-Higgs doublet models*, JHEP **07** (2013) 053 [arXiv:1302.4022] [INSPIRE].

[41] C.-W. Chiang and K. Yagyu, *Implications of Higgs boson search data on the two-Higgs doublet models with a softly broken Z_2 symmetry*, JHEP **07** (2013) 160 [arXiv:1303.0168] [INSPIRE].

[42] B. Grinstein and P. Uttayarat, *Carving out parameter space in type-II two Higgs doublets model*, JHEP **06** (2013) 094 [*Erratum ibid.* **09** (2013) 110] [arXiv:1304.0028] [INSPIRE].

[43] C.-Y. Chen, S. Dawson and M. Sher, *Heavy Higgs searches and constraints on two Higgs doublet models*, Phys. Rev. **D 88** (2013) 015018 [arXiv:1305.1624] [INSPIRE].

[44] O. Eberhardt, U. Nierste and M. Wiebusch, *Status of the two-Higgs-doublet model of type-II*, JHEP **07** (2013) 118 [arXiv:1305.1649] [INSPIRE].

[45] N. Craig, J. Galloway and S. Thomas, *Searching for signs of the second Higgs doublet*, arXiv:1305.2424 [INSPIRE].

[46] G. Bélanger, B. Dumont, U. Ellwanger, J.F. Gunion and S. Kraml, *Global fit to Higgs signal strengths and couplings and implications for extended Higgs sectors*, Phys. Rev. **D 88** (2013) 075008 [arXiv:1306.2941] [INSPIRE].

[47] D. López-Val, T. Plehn and M. Rauch, *Measuring extended Higgs sectors as a consistent free couplings model*, JHEP **10** (2013) 134 [arXiv:1308.1979] [INSPIRE].

[48] V. Barger, L.L. Everett, H.E. Logan and G. Shaughnessy, *Scrutinizing the 125 GeV Higgs boson in two Higgs doublet models at the LHC, ILC and Muon Collider*, Phys. Rev. **D 88** (2013) 115003 [arXiv:1308.0052] [INSPIRE].

[49] S. Choi, S. Jung and P. Ko, *Implications of LHC data on 125 GeV Higgs-like boson for the standard model and its various extensions*, JHEP **10** (2013) 225 [arXiv:1307.3948] [INSPIRE].

[50] S. Chang et al., *Two Higgs doublet models for the LHC Higgs boson data at* $\sqrt{s} = 7$ *and* 8 *TeV*, arXiv:1310.3374 [INSPIRE].

[51] K. Cheung, J.S. Lee and P.-Y. Tseng, *Higgcision in the two-Higgs doublet models*, *JHEP* **01** (2014) 085 [arXiv:1310.3937] [INSPIRE].

[52] J.R. Espinosa, C. Grojean, V. Sanz and M. Trott, *NSUSY fits*, *JHEP* **12** (2012) 077 [arXiv:1207.7355] [INSPIRE].

[53] A. Azatov, S. Chang, N. Craig and J. Galloway, *Higgs fits preference for suppressed down-type couplings: implications for supersymmetry*, *Phys. Rev.* **D 86** (2012) 075033 [arXiv:1206.1058] [INSPIRE].

[54] P. Bechtle et al., *MSSM interpretations of the LHC discovery: light or heavy Higgs?*, *Eur. Phys. J.* **C 73** (2013) 2354 [arXiv:1211.1955] [INSPIRE].

[55] J. Cao, Z. Heng, J.M. Yang and J. Zhu, *Status of low energy SUSY models confronted with the LHC 125 GeV Higgs data*, *JHEP* **10** (2012) 079 [arXiv:1207.3698] [INSPIRE].

[56] H. Baer et al., *Post-LHC7 fine-tuning in the mSUGRA/CMSSM model with a 125 GeV Higgs boson*, *Phys. Rev.* **D 87** (2013) 035017 [arXiv:1210.3019] [INSPIRE].

[57] P.W. Higgs, *Broken symmetries and the masses of gauge bosons*, *Phys. Rev. Lett.* **13** (1964) 508 [INSPIRE].

[58] F. Englert and R. Brout, *Broken symmetry and the mass of gauge vector mesons*, *Phys. Rev. Lett.* **13** (1964) 321 [INSPIRE].

[59] G.S. Guralnik, C.R. Hagen and T.W.B. Kibble, *Global conservation laws and massless particles*, *Phys. Rev. Lett.* **13** (1964) 585 [INSPIRE].

[60] ATLAS collaboration, *Measurements of the properties of the Higgs-like boson in the two photon decay channel with the ATLAS detector using 25 fb*$^{-1}$ *of proton-proton collision data*, ATLAS-CONF-2013-012 (2013).

[61] ATLAS collaboration, *Combined coupling measurements of the Higgs-like boson with the ATLAS detector using up to 25 fb*$^{-1}$ *of proton-proton collision data*, ATLAS-CONF-2013-034 (2013).

[62] ATLAS collaboration, *Search for the bb decay of the standard model Higgs boson in associated W/ZH production with the ATLAS detector*, ATLAS-CONF-2013-079 (2013).

[63] ATLAS collaboration, *Evidence for Higgs boson decays to the* $\tau^+\tau^-$ *final state with the ATLAS detector*, ATLAS-CONF-2013-108 (2013).

[64] CMS collaboration, *Updated measurements of the Higgs boson at 125 GeV in the two photon decay channel*, CMS-PAS-HIG-13-001 (2013).

[65] CMS collaboration, *Properties of the Higgs-like boson in the decay* $H \to ZZ \to 4l$ *in pp collisions at* $\sqrt{s} = 7$ *and* 8 *TeV*, CMS-PAS-HIG-13-002 (2013).

[66] CMS collaboration, *Update on the search for the standard model Higgs boson in pp collisions at the LHC decaying to* W^+W^- *in the fully leptonic final state*, CMS-PAS-HIG-13-003 (2013).

[67] CMS collaboration, *Search for the standard-model Higgs boson decaying to tau pairs in proton-proton collisions at* $\sqrt{s} = 7$ *and* 8 *TeV*, CMS-PAS-HIG-13-004 (2013).

[68] CMS collaboration, *Search for the standard-model Higgs boson decaying to* $\tau\tau$ *in non VH channels*, CMS PAS HIG-13-004 Update, https://twiki.cern.ch/twiki/bin/view/CMSPublic/Hig13004TWikiUpdate.

JHEP06(2014)149

[69] CMS collaboration, *Search for the standard model Higgs boson produced in association with W or Z bosons, and decaying to bottom quarks*, CMS-PAS-HIG-13-012 (2013).

[70] CMS collaboration, *Combination of search results for Higgs boson production in association with a top-quark pair*, https://twiki.cern.ch/twiki/bin/view/CMSPublic/ttHCombinationTWiki.

[71] A. Juste, *Standard model Higgs boson searches at the Tevatron*, talk given at the *Hadron Collider Physics Symposium 2012*, Kyoto Japan, 15 Nov 2012, http://kds.kek.jp/conferenceDisplay.py?confId=9237.

[72] Y. Enari, *$H \to b\bar{b}$ from Tevatron*, talk given at the *Hadron Collider Physics Symposium 2012*, Kyoto Japan, 14 Nov 2012, http://kds.kek.jp/conferenceDisplay.py?confId=10808.

[73] CMS collaboration, *Study of the mass and spin-parity of the Higgs boson candidate via its decays to Z boson pairs*, *Phys. Rev. Lett.* **110** (2013) 081803 [arXiv:1212.6639] [INSPIRE].

[74] ATLAS collaboration, *Evidence for the spin-0 nature of the Higgs boson using ATLAS data*, *Phys. Lett.* **B 726** (2013) 120 [arXiv:1307.1432] [INSPIRE].

[75] B.C. Regan, E.D. Commins, C.J. Schmidt and D. DeMille, *New limit on the electron electric dipole moment*, *Phys. Rev. Lett.* **88** (2002) 071805 [INSPIRE].

[76] C.A. Baker et al., *An improved experimental limit on the electric dipole moment of the neutron*, *Phys. Rev. Lett.* **97** (2006) 131801 [hep-ex/0602020] [INSPIRE].

[77] W.C. Griffith et al., *Improved limit on the permanent electric dipole moment of ^{199}Hg*, *Phys. Rev. Lett.* **102** (2009) 101601 [INSPIRE].

[78] ACME collaboration, J. Baron et al., *Order of magnitude smaller limit on the electric dipole moment of the electron*, *Science* **343** (2014) 269 [arXiv:1310.7534] [INSPIRE].

[79] J. Shu and Y. Zhang, *Impact of a CP-violating Higgs sector: from LHC to baryogenesis*, *Phys. Rev. Lett.* **111** (2013) 091801 [arXiv:1304.0773] [INSPIRE].

[80] J. Brod, U. Haisch and J. Zupan, *Constraints on CP-violating Higgs couplings to the third generation*, *JHEP* **11** (2013) 180 [arXiv:1310.1385] [INSPIRE].

[81] J.R. Ellis, J.S. Lee and A. Pilaftsis, *Electric dipole moments in the MSSM reloaded*, *JHEP* **10** (2008) 049 [arXiv:0808.1819] [INSPIRE].

[82] J. Ellis, J.S. Lee and A. Pilaftsis, *A geometric approach to CP-violation: applications to the MCPMFV SUSY model*, *JHEP* **10** (2010) 049 [arXiv:1006.3087] [INSPIRE].

[83] J. Ellis, J.S. Lee and A. Pilaftsis, *Maximal electric dipole moments of nuclei with enhanced Schiff moments*, *JHEP* **02** (2011) 045 [arXiv:1101.3529] [INSPIRE].

[84] K. Cheung, T.-J. Hou, J.S. Lee and E. Senaha, *Higgs mediated EDMs in the next-to-MSSM: an application to electroweak baryogenesis*, *Phys. Rev.* **D 84** (2011) 015002 [arXiv:1102.5679] [INSPIRE].

[85] D.A. Dicus, *Neutron electric dipole moment from charged Higgs exchange*, *Phys. Rev.* **D 41** (1990) 999 [INSPIRE].

[86] G.F. Giudice and A. Romanino, *Electric dipole moments in split supersymmetry*, *Phys. Lett.* **B 634** (2006) 307 [hep-ph/0510197] [INSPIRE].

[87] Y. Li, S. Profumo and M. Ramsey-Musolf, *Higgs-Higgsino-gaugino induced two loop electric dipole moments*, *Phys. Rev.* **D 78** (2008) 075009 [arXiv:0806.2693] [INSPIRE].

[88] T. Abe, J. Hisano, T. Kitahara and K. Tobioka, *Gauge invariant Barr-Zee type contributions to fermionic EDMs in the two-Higgs doublet models*, *JHEP* **01** (2014) 106 [arXiv:1311.4704] [INSPIRE].

JHEP06(2014)149

[89] S.M. Barr and A. Zee, *Electric dipole moment of the electron and of the neutron*, *Phys. Rev. Lett.* **65** (1990) 21 [*Erratum ibid.* **65** (1990) 2920] [INSPIRE].

[90] I.B. Khriplovich and S.K. Lamoreaux, *CP violation without strangeness*, Springer, New York U.S.A. (1997).

[91] M. Pospelov and A. Ritz, *Electric dipole moments as probes of new physics*, *Annals Phys.* **318** (2005) 119 [hep-ph/0504231] [INSPIRE].

[92] V.A. Dzuba, V.V. Flambaum and C. Harabati, *Relations between matrix elements of different weak interactions and interpretation of the parity-nonconserving and electron electric-dipole-moment measurements in atoms and molecules*, *Phys. Rev.* **A 84** (2011) 052108.

[93] M. Pospelov and A. Ritz, *Theta induced electric dipole moment of the neutron via QCD sum rules*, *Phys. Rev. Lett.* **83** (1999) 2526 [hep-ph/9904483] [INSPIRE].

[94] M. Pospelov and A. Ritz, *Theta vacua, QCD sum rules and the neutron electric dipole moment*, *Nucl. Phys.* **B 573** (2000) 177 [hep-ph/9908508] [INSPIRE].

[95] M. Pospelov and A. Ritz, *Neutron EDM from electric and chromoelectric dipole moments of quarks*, *Phys. Rev.* **D 63** (2001) 073015 [hep-ph/0010037] [INSPIRE].

[96] D.A. Demir, M. Pospelov and A. Ritz, *Hadronic EDMs, the Weinberg operator and light gluinos*, *Phys. Rev.* **D 67** (2003) 015007 [hep-ph/0208257] [INSPIRE].

[97] D.A. Demir, O. Lebedev, K.A. Olive, M. Pospelov and A. Ritz, *Electric dipole moments in the MSSM at large* $\tan\beta$, *Nucl. Phys.* **B 680** (2004) 339 [hep-ph/0311314] [INSPIRE].

[98] K.A. Olive, M. Pospelov, A. Ritz and Y. Santoso, *CP-odd phase correlations and electric dipole moments*, *Phys. Rev.* **D 72** (2005) 075001 [hep-ph/0506106] [INSPIRE].

[99] R.L. Arnowitt, J.L. Lopez and D.V. Nanopoulos, *Electric dipole moment of the neutron in supersymmetric theories*, *Phys. Rev.* **D 42** (1990) 2423 [INSPIRE].

[100] T. Ibrahim and P. Nath, *The neutron and the electron electric dipole moment in* $N=1$ *supergravity unification*, *Phys. Rev.* **D 57** (1998) 478 [*Erratum ibid.* **D 58** (1998) 019901] [*Erratum ibid.* **D 60** (1999) 079903] [*Erratum ibid.* **D 60** (1999) 119901] [hep-ph/9708456] [INSPIRE].

[101] O. Lebedev, K.A. Olive, M. Pospelov and A. Ritz, *Probing CP-violation with the deuteron electric dipole moment*, *Phys. Rev.* **D 70** (2004) 016003 [hep-ph/0402023] [INSPIRE].

[102] J. Engel, M. Bender, J. Dobaczewski, J.H. De Jesus and P. Olbratowski, *Time reversal violating schiff moment of* ^{225}*Ra*, *Phys. Rev.* **C 68** (2003) 025501 [nucl-th/0304075] [INSPIRE].

[103] EDM collaboration, Y.K. Semertzidis et al., *A new method for a sensitive deuteron EDM experiment*, *AIP Conf. Proc.* **698** (2004) 200 [hep-ex/0308063] [INSPIRE].

[104] L. Willmann, K. Jungmann and H.W. Wilschut, *Searches for permanent electric dipole moments in radium isotopes. Letter of intent to the ISOLDE and Neutron Time-of-Flight Experiments Committee for experiments with HIE-ISOLDE*, CERN-INTC-2010-049, INTC-I-115 (2010).

[105] S. Inoue, M.J. Ramsey-Musolf and Y. Zhang, *CPV phenomenology of flavor conserving two Higgs doublet models*, arXiv:1403.4257 [INSPIRE].